


Article

Distribution, Sedimentology and Origin of Mineralogical Assemblages from a Continental Na-bentonite Deposit in the Cretaceous Neuquén Basin (Argentina)

Telma Belén Musso^{1,2}, Gisela Pettinari^{1,2}, Manuel Pozo^{3,*} , Alexis Gabriel Martínez⁴ and Rafael González⁵

¹ Instituto de Investigación y Desarrollo en Ingeniería de Procesos, Biotecnología y Energías Alternativas, PROBIEN (CONICET-UNCo), Universidad Nacional del Comahue, Buenos Aires 1400, Neuquén, Argentina; telma.musso@probien.gob.ar (T.B.M.); gisela.pettinari@probien.gob.ar (G.P.)

² Departamento de Geología y Petróleo, Facultad de Ingeniería, Universidad Nacional del Comahue, Buenos Aires 1400, Neuquén, Argentina

³ Department of Geology and Geochemistry, Faculty of Sciences, Autonomous University of Madrid, Campus de Cantoblanco, 28049 Madrid, Spain

⁴ Tolsa Minerales La Patagonia S.A. Parque Industrial, Cinco Saltos 8303, Río Negro, Argentina; alexis.martinez@tolsa.com

⁵ Tolsa S.A., Carretera de Madrid a Rivas Jarama 35, 28031 Madrid, Spain; rgonzalez@tolsa.com

* Correspondence: manuel.pozo@uam.es

Abstract: Collected samples of bentonite and associated facies from the Justina deposit of Cretaceous age (Anacleto Formation) have been studied. Facies analysis, mineralogical, and geochemical studies have been carried out using several techniques, including: XRD, FTIR, DTA-TGA, microscopy (OM, SEM-EDX), and chemical analysis. The deposit occurs in a shallow, saline lacustrine environment developed over a fluvial floodplain, with a thickness between 0.21 and 0.8 m intercalated between fine-grained siliciclastic facies. Three mineral assemblages were found. In assemblage 1, the bentonite has low content of detrital minerals and the smectite is sodic. In assemblage 2, the bentonite shows the occurrence of minor analcime and mica, slightly higher detrital mineral content and the smectite is sodic to sodic-calcic. The associated detrital facies (assemblage 3) is dominated by illite and a mixed layer of illite and calcic smectite (R0), subordinately kaolinite + chlorite, and locally low-ordered smectite. As inherited minerals are found: quartz, potassium feldspar, plagioclase, illite-mica, heavy minerals (monazite, zircon, apatite, titanomagnetite) and volcanic rock fragments (andesite, glass). Authigenic minerals are: sodium smectite, analcime, barite, celestine, gypsum, and hematite. A model for the formation of authigenic minerals is proposed, highlighting the formation of sodic smectite from the alteration of volcanic glass of trachyandesitic composition.

Keywords: bentonite; Na-smectite; analcime; Cretaceous; lacustrine-palustrine environment; barite; celestine



check for updates

Citation: Musso, T.B.; Pettinari, G.; Pozo, M.; Martínez, A.G.; González, R. Distribution, Sedimentology and Origin of Mineralogical Assemblages from a Continental Na-bentonite Deposit in the Cretaceous Neuquén Basin (Argentina). *Minerals* **2022**, *12*, 467. <https://doi.org/10.3390/min12040467>

Academic Editor: Francesco Cavalcante

Received: 13 March 2022

Accepted: 9 April 2022

Published: 11 April 2022

Publisher's Note: MDPI stays neutral with regard to jurisdictional claims in published maps and institutional affiliations.



Copyright: © 2022 by the authors. Licensee MDPI, Basel, Switzerland. This article is an open access article distributed under the terms and conditions of the Creative Commons Attribution (CC BY) license (<https://creativecommons.org/licenses/by/4.0/>).

1. Introduction

Bentonites, which consist essentially of clay minerals of the smectite group, have a wide range of industrial uses such as ceramic, food technology, construction, pharmacology, impermeabilization, paper manufacturing, oil, and beverages clarification, among others [1]. The use of the bentonites in these applications can be attributed to several unique properties, including a large chemically active surface area, high cation exchange capacity, small particle size, colloidal behavior in aqueous media, and high swelling capacity. In Argentinian Northpatagonic region, industrial rocks have been one of the main mineral resources, being continuously mined for more than four decades. The bentonite deposits of the Neuquén Basin together with those outcropping in the Cuyo Provinces represent the most important bentonite districts of Argentina. The classical deposits in Neuquén Basin can be grouped into two mining districts located in different lithostratigraphic units:

Cerro Bandera Formation (Upper Oligocene-Miocene) and Allen Formation (Upper Cretaceous) [2]. Cerro Bandera Formation is constituted by tuffs, sandy tuffs, and sandstones deposited in a fluvial environment, intercalated with lacustrine claystones [3]. On the other hand, Cretaceous bentonites belong to the Facies Association C of Allen Formation (Malargue Group), characterized by the alternation of greenish olive mudstones and thin lenticular beds of light green feldspathic sandstones, which corresponds to a littoral transitional marine sedimentary sequence [4]. It is generally agreed that the Allen Formation and Cerro Bandera Formation bentonites have formed by in-situ alteration of volcanic ash in low energy aqueous environments [2]. These beds of bentonite occur with tabular geometry and are mostly lying horizontally. Most of them contain sodium as their main interlayer cation and have very good rheological, binder, and adsorptive properties that make them suitable to be used in foundry and petroleum industry as well as isolating barriers and ceramic [2,5].

In Argentina, the bentonite deposits originated in continental settings are of Triassic and Neogene age and belong to: Fm. Potrerillos-Fm Cacheuta (Mendoza), Fm. Cortaderita -Fm. Barreal (San Juan) [6–8], Fm. Cerro Bandera (Neuquén) [9] and Fm Sarmiento (Chubut) [10]. Regarding Triassic-aged deposits, sodic bentonites have been identified, formed in a continental environment that includes alluvial, fluvial, and lacustrine deposits [8]. The beds with the highest proportion of smectite (up to 85%) are associated with ash-fall tuffs intercalated in the black shales of the Cacheuta Formation. The bentonite is yellowish grey in colour and can be up to 50 cm thick, consisting of sodium montmorillonite and zeolites (analcime). The proposed origin of these minerals is authigenic, as a result of the alteration of volcanic glass from pyroclastic ash-fall deposits.

Worldwide, there are numerous examples of continental bentonite deposits such as Upper Cretaceous bentonites from Canada (Wapiti Formation) [11], Eocene-Oligocene bentonites from Texas (Jackson and Gueydan Groups) [12], Miocene bentonites from Turkey (Hancili Formation) [13], Miocene bentonites from Bavaria [14], bentonites of Tertiary age from Brazil [15] and the Miocene bentonites from the Madrid basin [16] (and references therein), among others.

Recently, a new type of sodium bentonite deposit of Cretaceous age has been recognized intercalated with detrital continental facies of the Neuquén basin [17]. The site is located at 87 km SE of “Rincon de los Sauces” city in Neuquén province and belongs to the mining district named Justina (TOLSA S.A.). The objective of the present work is to determine the distribution and origin of the Justina deposit bentonites in its paleoenvironmental context. The characterization of the mineralogical assemblages and their spatial variation, integrated with the geochemistry and textural features of the bentonites, will be relevant aspects in order to reach this objective. This study will contribute to a better understanding about the formation of natural Cretaceous Na-bentonites deposited in continental settings.

2. Geological Setting and Stratigraphy

The Justina bentonite deposit is located in Neuquén basin (Argentina) in the proximity of the well-known paleontological site Auca Mahuevo [18] near the Auca Mahuida volcanic complex (Figure 1A).

The bentonite occurs within the Anacleto Formation, the uppermost lithostratigraphic unit of the Neuquén Group (Cenomanian-Campanian) [19–21]. The Neuquén Group comprises a sequence of continental sediments deposited during the initial foreland stage of the Neuquén Basin [22], conforming three fining-upward fluvial cycles varying in thickness from 500 to 1300 m [21]. Within the study area, the Anacleto Formation contains approximately 70 m of fine-grained deposits, composed mainly of pelitic and very fine psamitic levels [23]. Pelitic levels consist of alternations of massive reddish-brown mudstones and siltstones, while yellowish to grayish-pink sandstones of medium- to fine-grained size conform the psamitic facies of the sequence. The lower boundary of this unit is not exposed, and the top is an unconformity overlaid by estuarine and shallow marine deposits of the Allen Formation (Malargüe Group) [23]. On the basis of palaeomagnetic studies, the age

proposed for this formation ranges between 83.5 and 74.5 Ma (lower to medium Campanian) [24]. The Anacleto Formation is up to 90 m thick, and the type locality is situated 50 km west of Neuquén city [23].

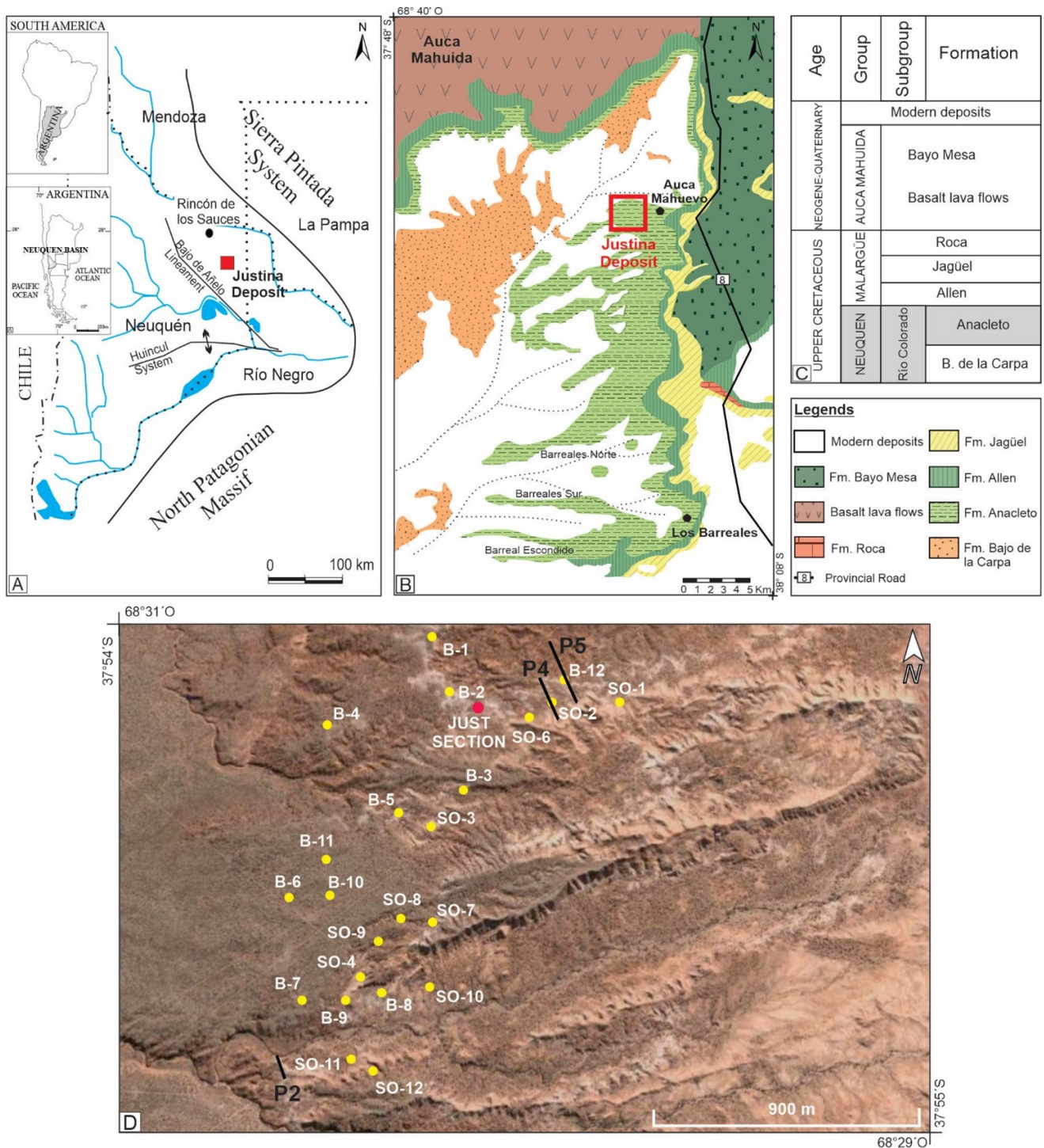


Figure 1. (A) Geographical location of the Neuquén basin and the study area. (B) Geological map of the study area and surroundings. (C) Stratigraphic table showing the Anacleto Formation. (D) Location of sampling points (B: trial pits; SO: boreholes), section JUST and described stratigraphic profiles (P).

According to [25], Anacleto Formation can be divided into two main sections in the study area. The 57 m thick lower section is constituted by fine-grained, mixed-load meandering river deposits in which overbank deposits conform more than 85% of outcrop thickness. The 17 m thick upper section exhibits a predominance of lacustrine, pond, and slough deposits, reflecting a shift toward more poorly drained floodplain. A transition to major aridity toward this part of the sequence is inferred from the presence of sandy levels cemented with gypsum.

From a structural point of view, the bentonite deposit is located in a depression called “Bajo de Añelo” which consists in a regional NW oriented feature (Figure 1B). In structural maps is clearly visible as a 750 m relief regional syncline. From SE to NW is divided into three segments in terms of their different morphology, subsidence drivers and structural evolution. The study area is located in the central segment of the “Bajo de Añelo”. In this region, the tectonic evolution was controlled, first, by a cortical attenuation in early Jurassic, which produced differential subsidence, and later, by the effects of Huincul System structure [26].

3. Materials and Methods

3.1. Fieldwork and Sampling

The interpretation of the sedimentological and paleoenvironmental conditions associated to the bentonite deposit was based on the facies description of one reference stratigraphic section (P5) and two representative stratigraphic sections from the south (P2) and north (P4) zones (Figure 1C). Lithofacies were defined using the criteria for fluvial facies [27]. Their analysis, together with the study of boundary surfaces and geometry of depositional units, allowed to define facies associations useful for recognition and interpretation of the depositional system [27,28]. In some cases, new nomenclature codes for lithofacies were created due to the absence of proper ones. These acronyms were: Htl (laminated heterolite) and B (bentonite). An additional code, named DO (distal overbank deposits), was also used for the identified facies association.

Twenty-three samples were collected for the mineralogical and chemical study of the bentonite: eleven from trial pits (B) and twelve from boreholes (SO) (Figure 1C). As can be seen, the distribution of the sampling points forms an alignment of the trial pits further west and the boreholes further east. An outcrop named section JUST was also sampled (4 samples) with the aim to study a sedimentological sequence as a reference that includes the bentonite and associated lithofacies (Figure 1C). A total of 8 bentonite samples (B-1, B-4, B-6, B-8, B-9, B-10, B-12, and JUST-2) had previously been mineralogically characterized by [17]. Seven samples from the lithofacies associated to the bottom and top of the bentonite level were added for their study (Figure 2). The bentonite is intercalated in siliciclastic facies and is easy to identify due to its grey to pink colors, sometimes showing red inserts in grey bentonite (Figure 3). The bentonite bed is horizontal to subhorizontal, 0.21–0.8 m thick (0.60 m average value), commonly displaying laminated structure.

3.2. Experimental Methodology

Mineralogical analysis of 19 samples was carried out by means of X-ray diffraction (XRD) in a Bruker D8 with Lynxeye XE-T detector equipment, using CuK α radiation (40 kV, 20 mA) and a scanning speed of 1° 2 θ /min. The powdered whole-rock samples were used to determine bulk mineralogy and complemented the results previously reported by [17]. After clay fraction separation (<2 μ m), 13 sample mounts were prepared from suspensions oriented on glass slides. The identification of the clay minerals was carried out on oriented mounts of air-dried sample, with ethylene glycol solvation, and heated at 550 °C. The mineral intensity factors (MIF) method was applied to XRD reflection intensity ratios normalized to 100% with calibration constants for the quantitative estimation of mineral contents [29–31]. To establish the relative ordering (“crystallinity”) of smectite, the FWHM (full width at half maximum) parameter was measured on the (001) reflection on ethylene glycol oriented mount [32]. The crystallite size was calculated using the Scherrer equation.

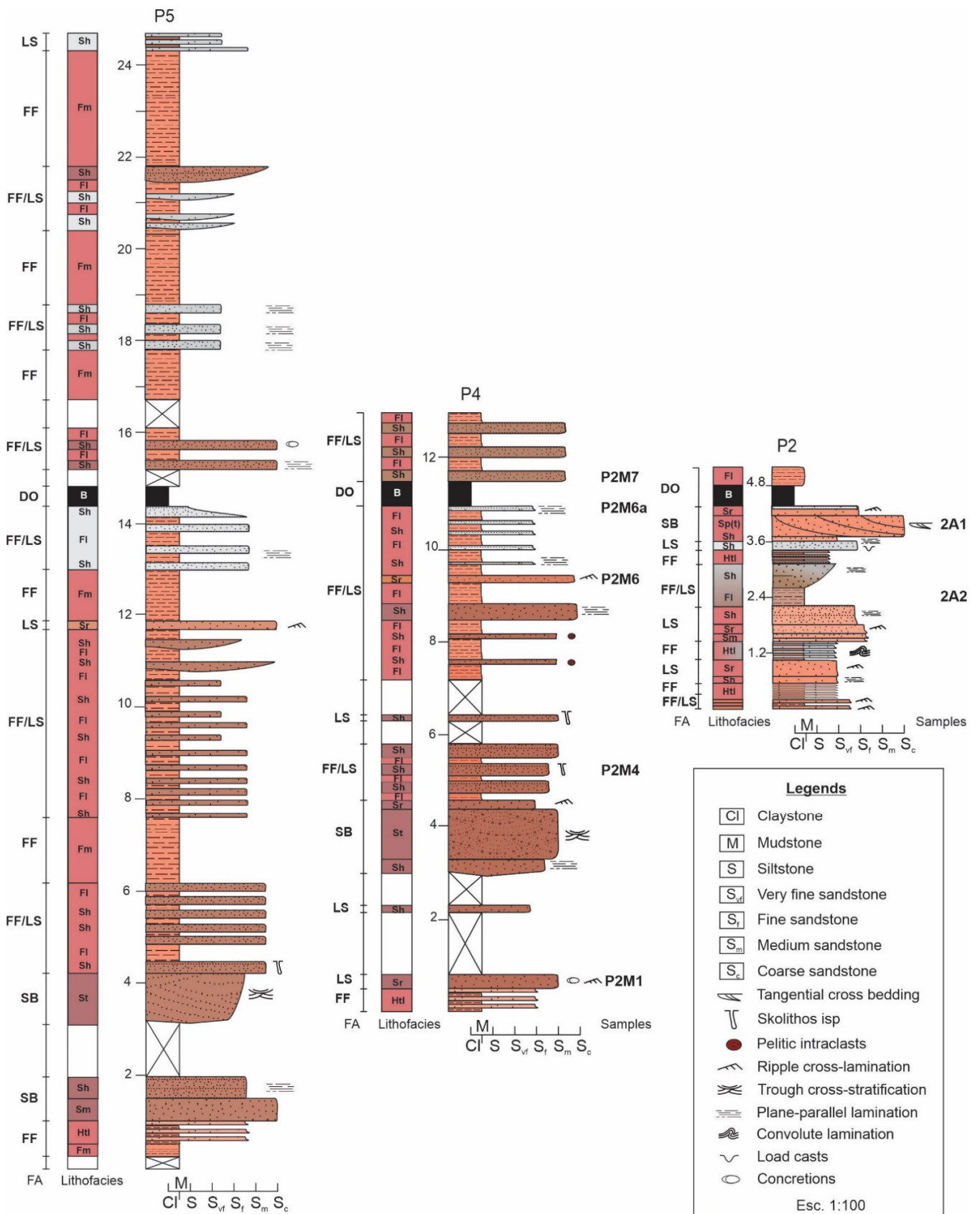


Figure 2. Stratigraphic profiles with location of the lithofacies and lithofacies associations identified in the Anacleto Formation for the studied area. Highlights the location of the bentonite bed (B).

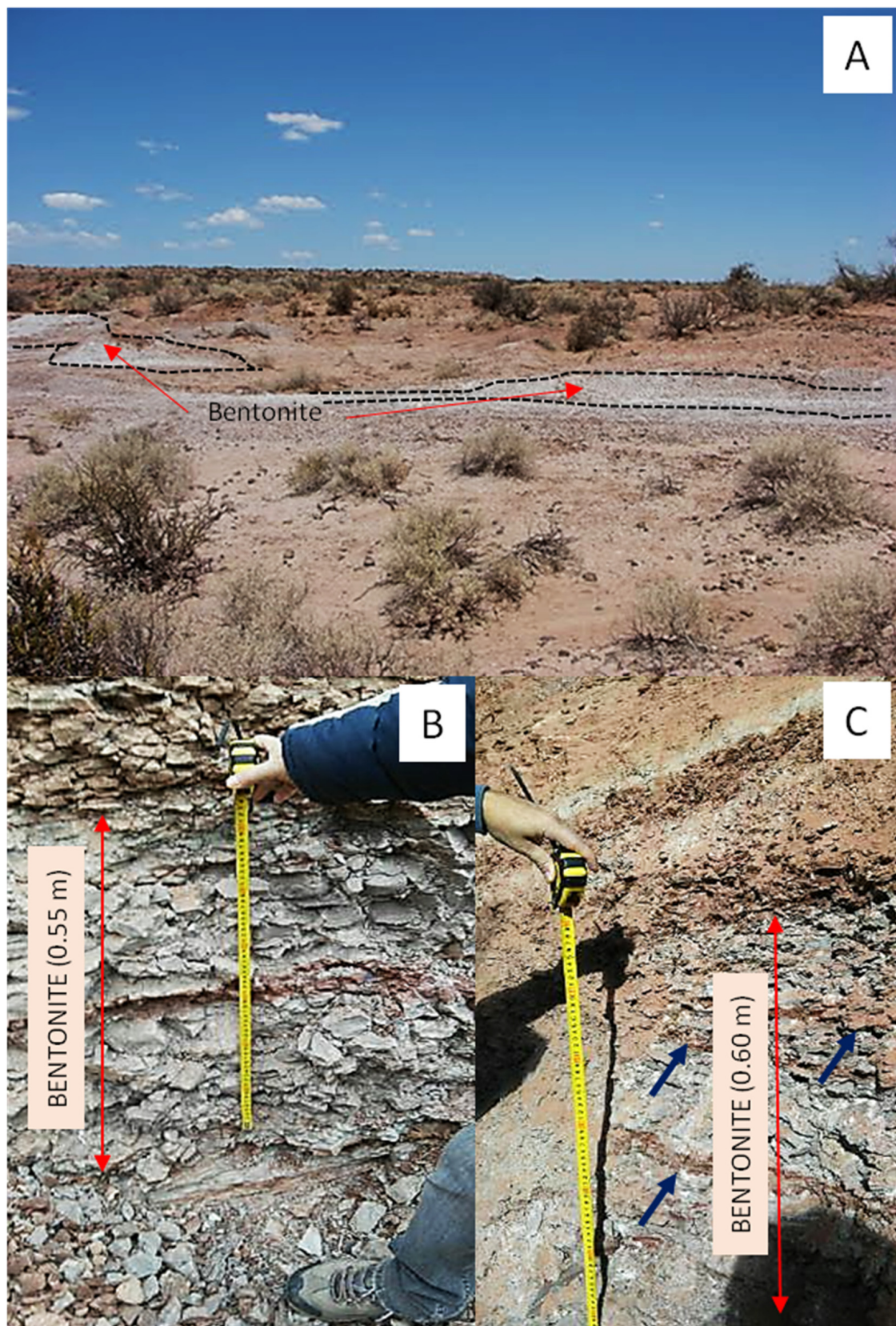


Figure 3. Fieldwork pictures of the Justina bentonite deposit. (A) Outcrop view of bentonite level easily recognized by their light color. (B) Trial pit showing bedded mostly grey bentonite overlying laminated greenish sandy siltstone (B-5). (C) Grey bentonite with inserts of red laminated bentonite (arrows) is common at some points (B-4).

The thermal analysis (DSC/DTA/TGA Q600 of TA Instruments, New Castle, DE, USA) of two representative samples was performed using 10 mg of powdered clay sample in a Pt sample holder at an average heating rate of 10 °C/min with an alumina reference. Infrared spectroscopy (FTIR) (Bruker IFS 66v standard) spectra of the same two representative samples were recorded with a spectral resolution of 2 cm⁻¹ in transmission mode in the region 400–4000 cm⁻¹. The samples were examined in KBr pellets (3 mg/300 mg KBr). Chemical analyses of 5 whole-rock bentonites were carried out using sample fusion and inductively coupled plasma atomic emission spectroscopy (ICP-AES and MS) for major and trace elements at ATLABS laboratories (Ancaster, ON, Canada). The detection limits for analyses were between 0.01 and 0.001 wt. % for major elements and between 0.05 and 30 ppm for trace elements. The results of major elements of three of them (B-1, B8 and B12) were previously reported in [17]. For comparison purpose, a representative sample from Pellegrini bentonite deposit (PEL) was also analysed.

A total of 4 selected broken samples were examined by backscattered electrons (BSE) scanning electron microscopy (S-3000N with detector ESED attached to EDX analyser of Oxford Instruments, ICAx-sight model, Oxfordshire, UK) after coating with gold (10 nm thick) in a sputtering chamber. In the descriptions of the microfabric of the samples examined, the terminology proposed by [33] was used. A representative bentonite sample (JUST-2) was described by petrographic techniques. The sample required epoxy consolidation before standard thin section could be made.

4. Results

4.1. Lithofacies Description

In the study area, the Anacleto Formation is comprised by sediments and sedimentary rocks, mainly detrital, consisting of sandstones and mudstones where bentonite deposit is inserted. The sedimentological profiles are situated in the lower section of Anacleto Formation [25] (Figure 2). Based on codes and definitions summarized by [27], eight lithofacies are recognized in the Anacleto Formation within the study area. The main features of these facies are summarized in Table 1 and Figure 4.

Table 1. Description and interpretation of the lithofacies defined in Anacleto Formation, according to the criteria and nomenclature by [27]. Munsell codes (Rock Colour Chart).

Code	Descriptions	Interpretations
Sh	Fine- to medium-grained sandstones, moderate reddish brown (10R 4/6), with horizontal stratification. Tabular bodies up to 45 cm thick and several meters of lateral extension. Net and planar base. Skolithos isp. trace fossils can be present.	Plane-bed deposits Upper flow regime
St	Fine- to medium-grained micaceous sandstones, moderate reddish-brown (10R 4/6) to moderate reddish-orange (10R 6/6), with medium scale trough cross stratification. Bodies of tabular and lenticular geometry up to 1 m thick, with net planar base.	3D bedforms (sandy dunes) Lower flow regime
Sr	Very fine- to medium-grained size micaceous sandstones, moderate reddish-brown (10R 4/6) to moderate reddish-orange (10R 6/6), with ripple cross-lamination. Bodies of tabular and lenticular geometry up to 34 cm thick, with net planar base. Scoyenia isp. trace fossils can be present.	3D ripples (linguoid dunes) Lower flow regime
Sp(t)	Medium- to coarse-grained sandstones, moderate reddish-brown (10R 4/6) to pale reddish-brown (10R 5/4), with tangential cross bedding. Tabular deposits up to 45 cm thick, with lateral wedge like geometry and several meters of extension. Net and planar base.	3D bedforms Lower flow regime

Table 1. Cont.

Code	Descriptions	Interpretations
Htl	Very fine-grained sandstones and mud, moderate reddish-brown (10R 4/6), with parallel lamination, in some cases associated to convolute lamination. Tabular bodies up to 49 cm thick, with laterally wedge like geometry and net planar base.	Tractive and decantation deposits associated to low regime unconfined flows. Saturated sediments deformed by load and density contrast.
Fl	Moderate brown (5YR 4/4) mudstones with plane-parallel lamination. Sheet-like deposits up to 45 cm thick, with net and planar base.	Deposition by decantation
Fm	Moderate brown (5YR 4/4) massive mudstones. Sheet-like deposits up to 2.5 m thick, with net and planar base.	Deposition by decantation
B	Light brownish-gray (5YR 6/1) to grayish red (10R 4/2) massive to laminated bentonite. Tabular bodies up to 55 cm thick, transitional base from lithofacies Fm-Fl. Remains of fossil leaves can be observed in red laminated bentonites.	Deposition by decantation, associated to shallow lakes

Psamitic lithofacies are constituted by texturally mature medium- to fine-grained size sandstones. Occasionally, abundant muscovite can be present with a variable content of mud matrix. In general, the deposits are thin (3–50 cm) and are subordinated to the mudstones. Exceptionally, sandstone strata can occur vertically stacked/amalgamated with thickness up to 2 m. These lithofacies were formed by unidirectional flows that developed typical bedforms, which indicate the predominance of tractive processes (lithofacies Sh, St, Sr, SP (t)) [27,34,35].

In the heterolithic lithofacies, there is a clear predominance of mudstones. This lithofacies is characterized by a milimetric to centimetric lamination of very fine-grained sandstones where can be also seen deformation structures such as convolute lamination. These deposits generate tabular bodies of rapid lateral wedging, with thicknesses of 50 cm to 1 m. Its development is subordinated in relation with the other fine-grained facies.

Fine grained facies predominate over psamitic facies and constitute a 65% of the analysed sequence. In general, the mudstones are in the form of poorly consolidated, reddish coloured, sheet-like bodies with several meters of lateral extension. The most frequent type is massive mudstones (Fm) followed by laminated mudstones (Fl). They can reach up to 2.5 m thick and both are related to deposition by decantation. The bentonite deposit (B) is a distinctive characteristic of this sequence. It is formed by a tabular level of 0.6 m thick (average value) and transitional boundaries with facies Fm-Fl, indicating that it is associated to a low energy depositional environment.

The reference stratigraphic sequence JUST constitutes a characteristic sedimentological sequence of the bentonite deposit (Figure 5). It is made up of a basal level of greenish sandy siltstone with a certain banded-laminated structure (JUST-1) on which the bentonite bed is laid out with the lower part (0.40 m) of grey colour (JUST-2), which passes upward to another with reddish inserts (JUST-3) (0.30 m), highlighting the presence of lamination and remains of fossil leaves in the reddish layer. At the top, it passes to a more reddish silty claystone level (0.20 m) with evidence of drab haloes and subaerial exposure in which evidence of root bioturbation has been recognised (JUST-4). Above this, there are reddish mudstones and fine-grained sandstones with bluish-green stains (0.50 m), cut and eroded by sandstones with laminated traction structures to top.

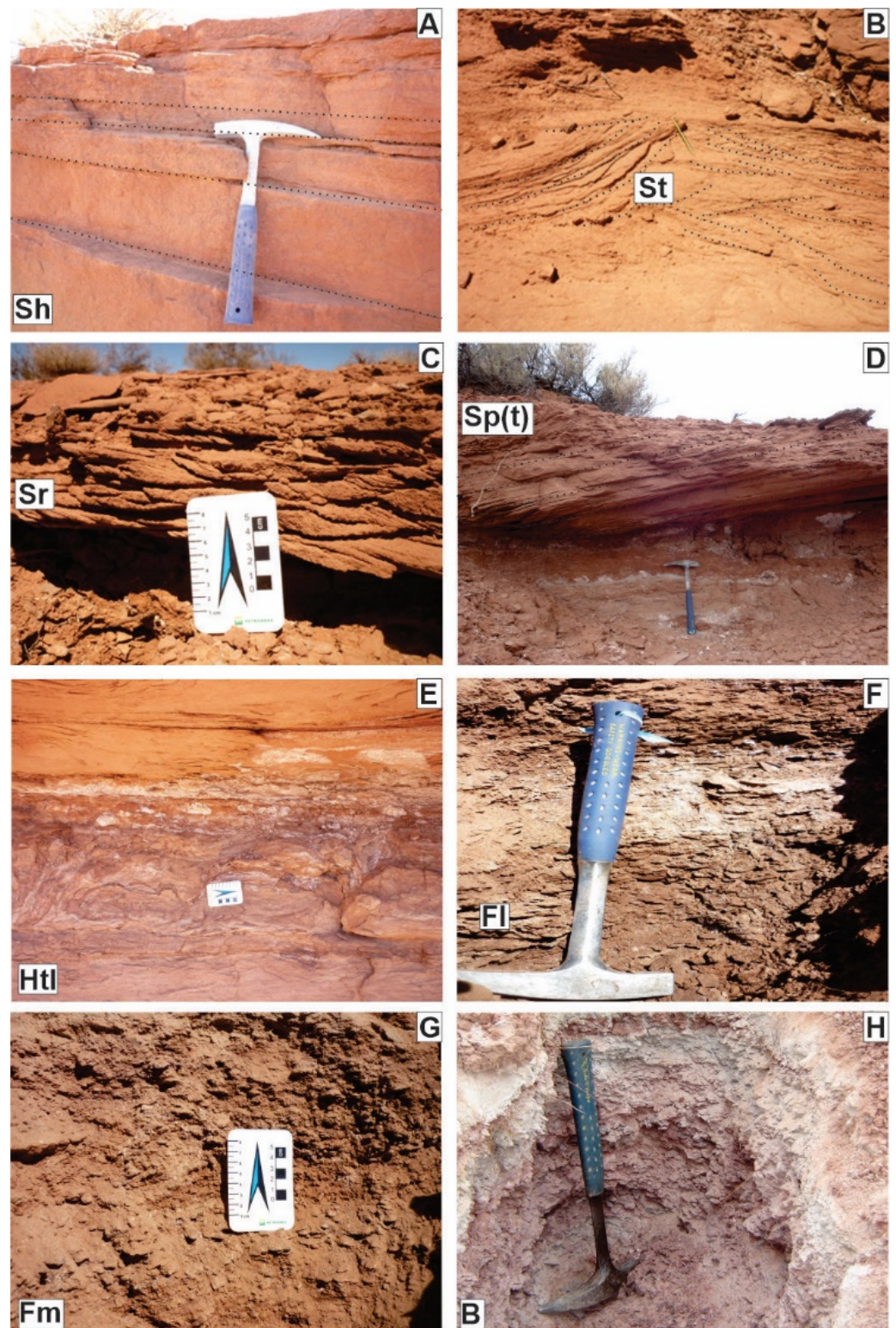


Figure 4. Photographs of the lithofacies defined in Anacleto Formation, according to the criteria and nomenclature by [27]. (A) Sh: plane bed deposits; (B) St: 3D bedforms (sandy dunes); (C) Sr: 3D ripples (linguoid dunes); (D) Sp(t): 3D bedforms; (E) Htl: Saturated sediments deformed by load and density contrast; (F) Fl: mudstones with plane-parallel lamination deposited by decantation; (G) Fm: massive mudstone deposited by decantation; (H) B: massive to laminated bentonite deposit.

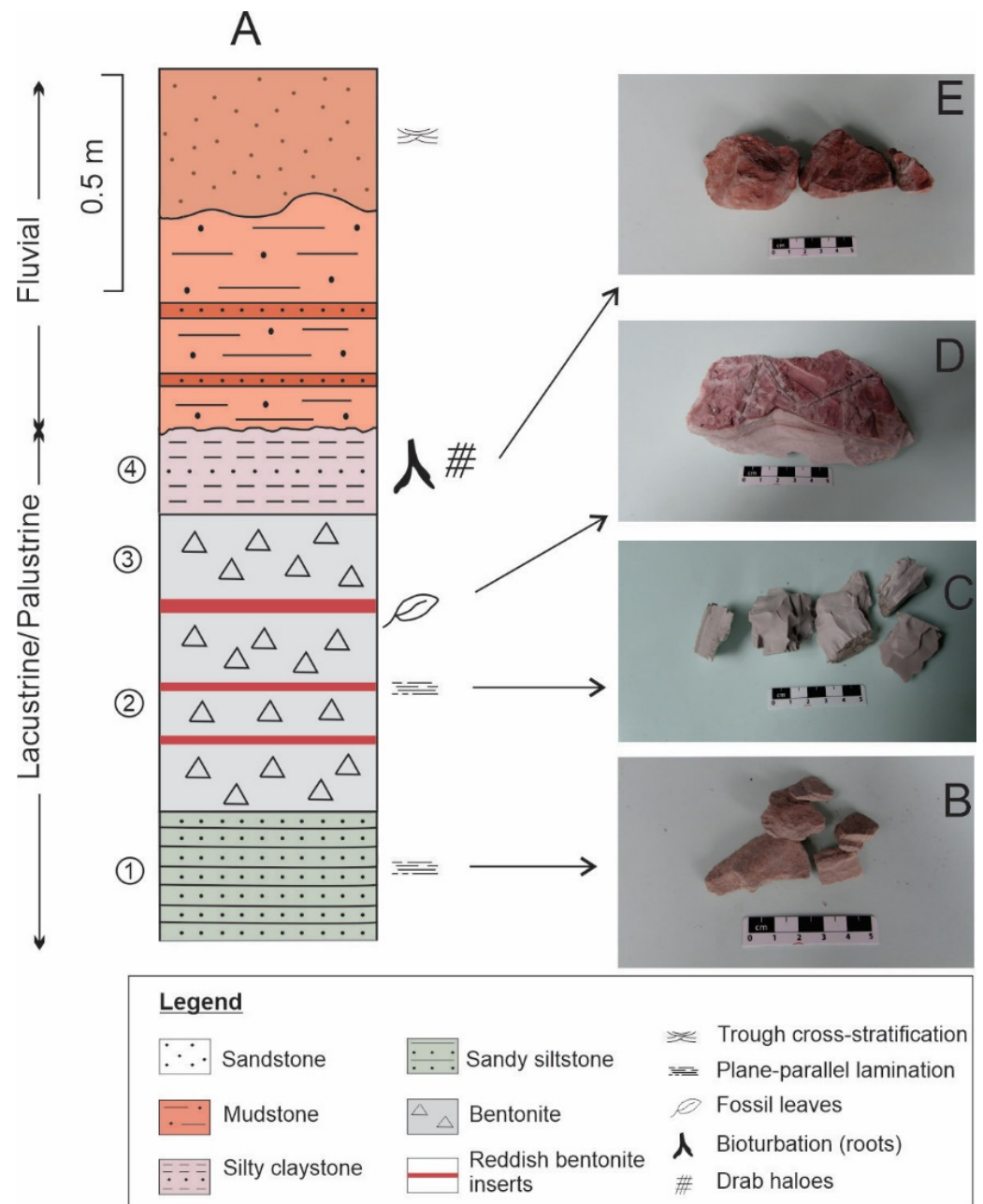


Figure 5. (A) Representative lithological sequence of the bentonite deposit showing a lacustrine-palustrine sequence overlaying by fluvial deposits. (B) Basal sandy siltstone displaying bedding-lamination (JUST-1). (C) Grey waxy bentonite (JUST-2). (D) Reddish bentonite laminated insert with plant remains (leaves) (JUST-3). (E) Silty claystone with palustrine features including reddening, drab haloes and root bioturbation (JUST-4).

According to trial pits (B) and borehole (SO) samples distribution, the topographic position of the bentonite is variable (Figure 6). In general, the beds are deeper towards the east with differences between the north zone (410 to 406 m) and the south zone (408–404). This mean that the top of the bentonite bed descends to the east and south of the study area.

4.2. Mineralogy

Mineralogical analysis was mainly performed by X-ray diffraction technique (XRD), which was complemented with infrared spectroscopy (FTIR), thermal analysis (DTA-TGA), petrography (grain mounts and thin sections), and scanning electron microscopy (SEM-EDX).

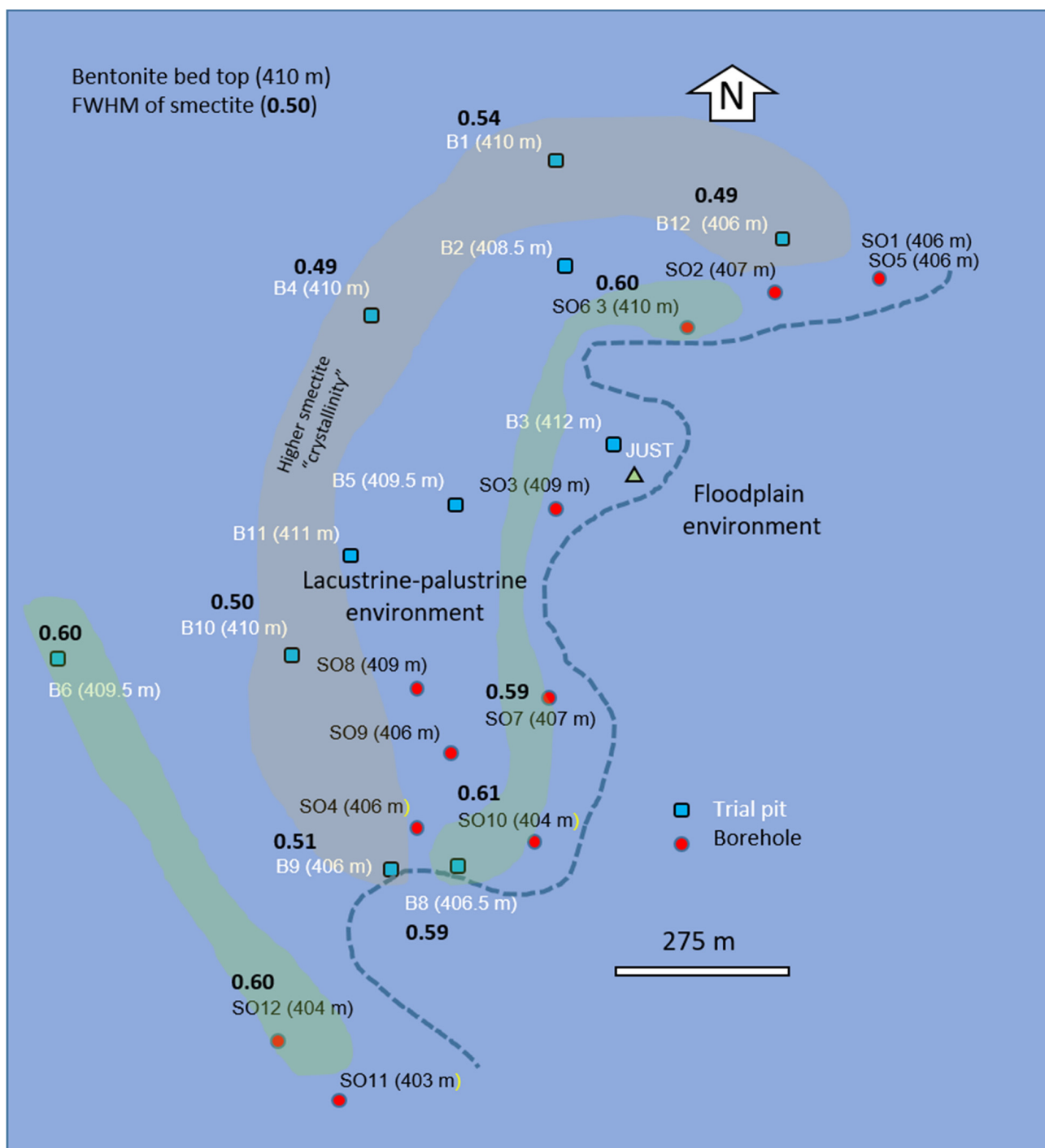


Figure 6. Map showing the topographic elevation of the bentonite bed top and the distribution of smectite FWHM values. The tentative boundary between fluvial and lacustrine facies is also indicated.

4.2.1. X-ray Diffraction

Mineralogical results from 25 samples from the bentonite deposit and 9 samples from the associated facies are shown in Table 2. In bentonites, phyllosilicates are dominant (74–98%) with a mean value of 92%. Quartz (1–7%) and feldspar (0–19%) occur subordinate with traces of gypsum and analcime (<2%). In the associated facies located below and upper the bentonite level, phyllosilicates content is variable (43–81%) and depends on the detrital minerals proportion such as feldspars (6–28%) and quartz (5–23%). In these lithologies is noticeably the presence of analcime reaching up to 7%, and mica in some samples.

Table 2. Bulk mineralogy (% *w/w*) of the bentonites and associated facies determined by XRD. Tr: traces. These results are complementary to those obtained and published in [17].

Lithology	Samples	Phyllosilicates	Quartz	Feldspars ¹	Gypsum	Analcime
Bentonite	B-2	90	4	4	2	0
Bentonite	B-3	96	2	1	1	0
Bentonite	B-5	88	4	7.5	0.5	0
Bentonite	B-11	93	3	2	2	0
Bentonite	SO-1	93	1.5	4	0.5	1
Bentonite	SO-2	86.7 *	4	7.5	0.5	0.75
Bentonite	SO-3	98	2	0	0	Id
Bentonite	SO-4	96 *	1.5	1.5	0	1
Bentonite	SO-5	96.5	1	1.5	0.5	0.5
Bentonite	SO-6	86.5 *	4.5	6.75	0.25	2
Bentonite	SO-7	86.5 *	4	9	Tr	0.5
Bentonite	SO-8	91.5 *	2.5	6	0	Tr
Bentonite	SO-9	95.5 *	2	2	0	0.5
Bentonite	SO-10	89 *	3	6.5	0	1.5
Bentonite	SO-11	74 *	7	19	0	Tr
Bentonite	SO-12	86.5 *	4	9.25	0	0.25
JUST section						
Silty claystone	JUST-4	81 *	5	6	0	7
Bentonite	JUST-3	99 *	1	0	0	0
Sandy siltstone	JUST-1	43.5 *	23	28	0.5	5

* Mica identified, ¹ K-feldspar + plagioclase.

The clay fraction (<2 µm) is mainly composed by smectite (>95%), which is frequently the only mineral present. In some cases, traces of illite can be detected (Table 3). The oriented clay mounts show the presence of Al-smectite ($d_{060} = 1.49\text{--}1.50 \text{ \AA}$) with Na as the main interlayer cation ($d_{001} = 12.5 \text{ \AA}$). The characteristics basal d-spacings of ethylene glycol solvated samples are: 16.96 Å (001), 8.45 Å (002), 5.60 Å (003), 4.22 Å (004), and 3.36 Å (005). According to [17] the smectite is Na-montmorillonite with the following crystallochemical formula: $(\text{Ca}_{0.13}, \text{Na}_{0.52}, \text{K}_{0.01}) (\text{Si}_{7.61}, \text{Al}_{0.38}) (\text{Al}_{2.84}, \text{Fe}^{3+}_{0.11}, \text{Mg}_{1.32}, \text{Ti}_{0.008}) \text{O}_{20}(\text{OH})_4$.

In the samples with the code (SO) can be observed a predominance of Ca ($d_{001} = 14\text{--}14.5 \text{ \AA}$) or a heterogeneous composition of the interlayer space with Ca and Na ($d_{001} = 13.08\text{--}13.81 \text{ \AA}$).

The FWHM parameter of the smectites is variable in the bentonite samples ranging from 0.59 to 0.61 2θ (Scherrer crystallite size around 14 nm) while in the associated silty claystone (JUST-4) this value is higher, indicating a poorer “crystallinity” (0.9 2θ, 9.59 nm). These FWHM values of bentonites are higher than those reported by [17] that commonly are lower than 0.60 with crystallite size reaching 17 nm.

The XRD study of the coarse silt fraction (53 µm) of bentonites showed the following relative abundance order: quartz > plagioclase > mica > K feldspar.

In the sandstone and mudstone samples, related to the bentonite bed, the clay mineralogy shows the presence of illite (15–73%) and a mixed-layer illite-smectite (R0) (23–87%) in which the swelling phase is calcic and represents between 50–70% of the same. In the identification of the mixed layer, the criteria of [32] have been followed. More subordinate phases (0–20%) are also identified at 7 Å (chlorite + kaolinite). In sample JUST-1, the coexistence of a Ca-smectite phase (linked to the illite-smectite mixed layer) and a discrete Na-smectite is outstanding.

Table 3. Clay mineralogy (<2 μm) (% *w/w*) of the bentonites and associated facies determined by XRD. FWHM ($^{\circ}2\theta$) and Scherrer crystallite sizes (Cr) (nm) values are also shown. Tr: traces. These results are complementary to those obtained and published in [17].

Sample	Lithology	Smectite	Illite	Kaol + Chlo	FWHM	Cr (nm)
SO-6	Bentonite	100	0	0	0.60	14.38
SO-7	Bentonite	100	0	0	0.59	14.63
SO-10	Bentonite	100	0	0	0.61	14.15
SO-12	Bentonite	100	Tr	0	0.60	14.38
JUST-4	Silty claystone	100	Tr	0	0.90	9.59
JUST-1	Sandy siltstone	98	2	Tr	1.06	8.14

Sample	Lithology	Mixed layers (I/Sm)	Illite	Kaol + Chlo
2A1	Sandstone	32 (Sm ₅₀)	48	20
2A2	Mudstone	48 (Sm ₇₀)	48	3
P2M7	Sandstone	45 (Sm ₅₀)	49	6
P2M6a	Sandstone	87 (Sm ₅₀)	13	Tr
P2M6	Sandstone	72 (Sm ₅₀)	26	2
P2M4	Sandstone	23 (Sm ₅₀)	73	4
P2M1	Sandstone	85 (Sm ₅₀)	15	0

Taking into account the bulk and clay mineralogy, three mineralogical assemblages were established (Figure 7):

Assemblage 1. Sodium dioctahedral smectite with low proportion of quartz, feldspars, and gypsum. The smectite is relatively well ordered (lower FWHM, larger crystallite size). Comprises the samples with the code B and JUST-2, 3.

Assemblage 2. Sodium, calcium, or Ca-Na dioctahedral smectite with variable proportion of quartz, feldspars, gypsum, mica, and analcime. The smectite is poorer ordered than that of assemblage 1 (higher FWHM, smaller crystallite size). Comprises the samples with the code SO and JUST-4.

Assemblage 3. Mixed layers illite-smectite R0 (50–70% Ca-smectite), illite, and subordinate 7 Å phases (chlorite + kaolinite). Comprises sandstones and mudstones from siliciclastic lithofacies and JUST-1.

4.2.2. Infrared Spectroscopy

The infrared spectroscopy and the spectral data of one representative bentonite (SO-3) and one silty claystone (JUST-4) is presented in Figure 8. Main differences between these samples are observed in the band region 900–400 cm^{-1} . Most of the bands such as 3622, 3436, 1640, 1030, 912, 836, 520, 468 cm^{-1} show the presence of montmorillonite [36,37]. The band at 3621 cm^{-1} corresponds to the stretching vibration of structural hydroxyl groups coordinated in the octahedral layer to Al + Mg. The band at 3436 cm^{-1} is due to OH stretching of water. The band that runs between 1600 and 1700 cm^{-1} is attributed to the vibrations of valence of the OH group of water constitution. The band towards 1639–1642 cm^{-1} is attributed to the vibrations of deformation of the H₂O molecules adsorbed between the layers. The intense band at 1028–1030 cm^{-1} corresponds to the stretching vibrations of Si-O.

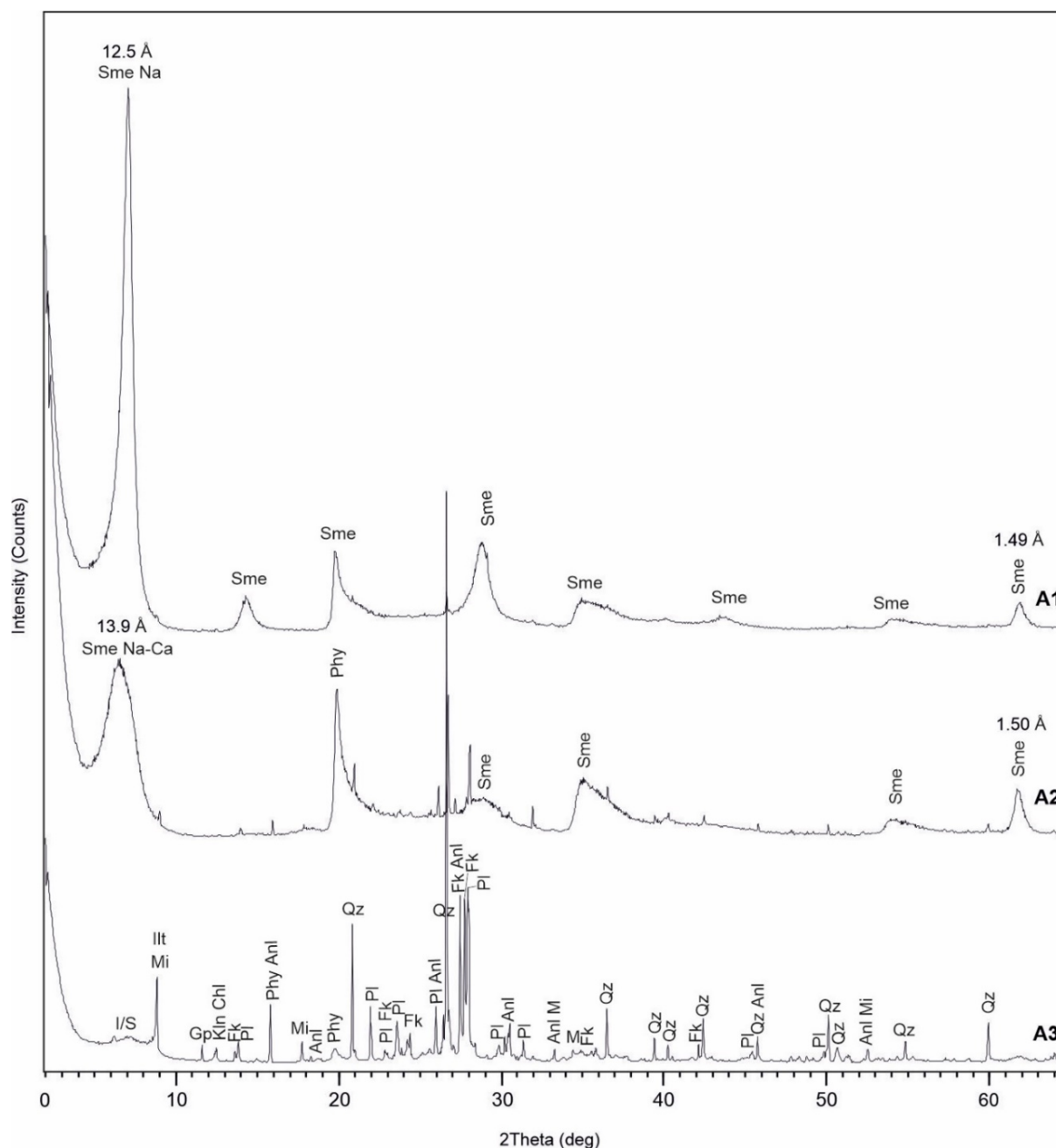


Figure 7. A1: Assemblage 1: Sodium smectite, quartz, feldspars, and gypsum. A2: Assemblage 2: Sodium, calcium, or Ca-Na smectite, quartz, feldspars, gypsum, mica, and analcime. A3: Assemblage 3: mixed layers Illite-smectite R0 (50–70% Ca-smectite), illite and chlorite + kaolinite. I/S: mixed layers Illite-smectite, M: mica, Ill: illite, Gp: gypsum, Kln + Chl: kaolinite + chlorite, Fk: alkaline feldspar, Pl: plagioclase, Phy: phyllosilicate Anl: analcime, Qz: quartz, Sme Na-Ca: smectite sodium-calcium, Sme Na: sodium smectite.

Two bands at 912 ($\delta(\text{Al}_2\text{OH})$) and 838 cm^{-1} ($\delta(\text{AlMgOH})$) reflect substantial substitution of octahedral Al by Mg in SO-3 montmorillonite [38]. However, this would not be the situation in JUST-4 where these bands are very weak (Figure 8). The bands at 778 cm^{-1} and 646 cm^{-1} are only present in JUST-4. Main mineralogical differences between this sample and SO-3 are related to its higher presence of quartz and the presence of analcime and feldspars (Table 2). In analcime, the band at 720–790 cm^{-1} and the band around 649 cm^{-1} have been described as associated with symmetric stretching vibration of 4-membered rings of silicate chains [39,40]. The band at 778 cm^{-1} can be also assigned to the Si-O stretching

of quartz as this sample has a higher quartz content, while the band at 649 cm^{-1} can also be due to the presence of K-feldspar [41].

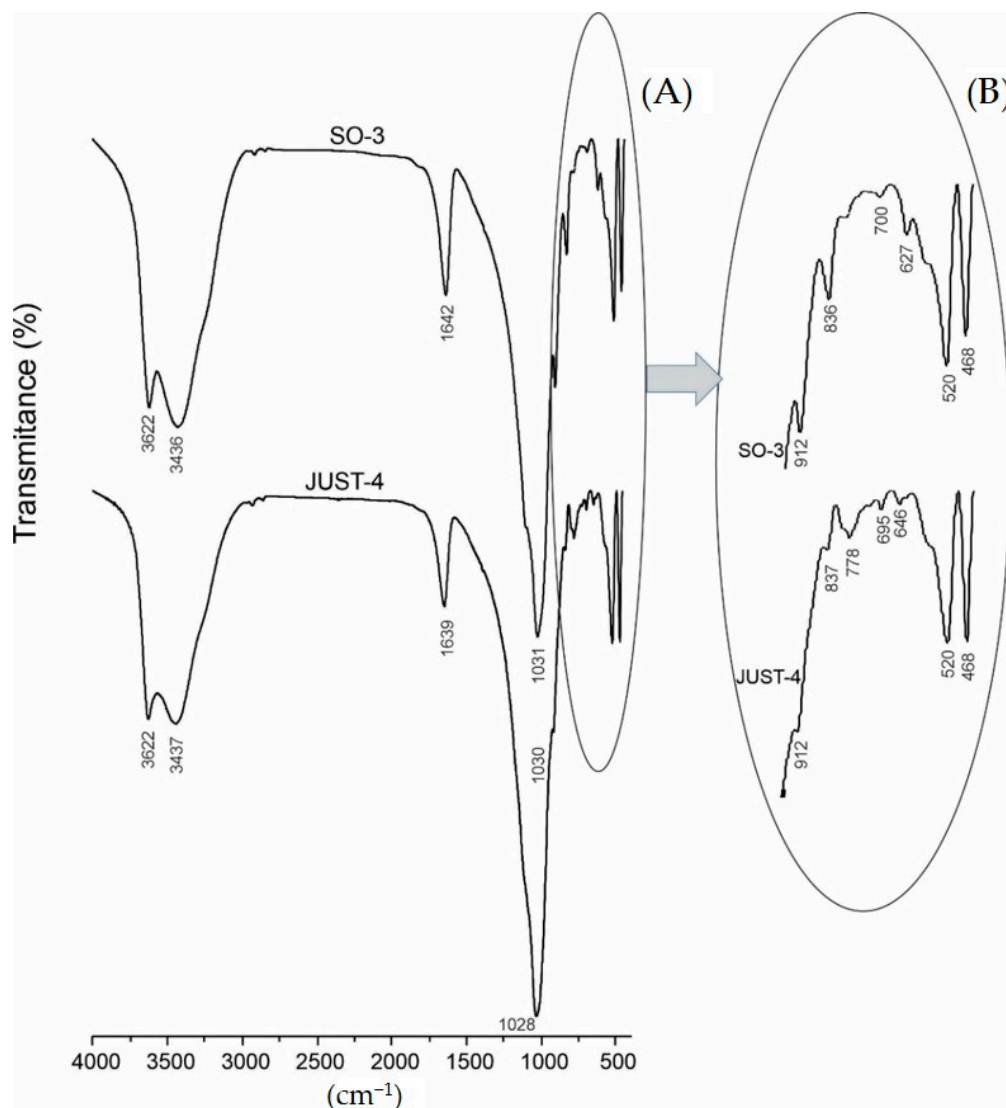


Figure 8. (A) FT-IR spectra of one representative bentonite (SO-3) and one silty claystone (JUST-4). (B) Detail of the $900\text{--}450\text{ cm}^{-1}$ range.

The band at 700 cm^{-1} is due to the deformation and bending modes of the Si-O bond. The band near 620 cm^{-1} due to coupled Al-O out-of-plane and Si-O vibrations is also characteristic for montmorillonite. The AlVI-O-Si bending band (AlVI-Al in octahedral positions) appears near 520 cm^{-1} and Si-O-Si near 470 cm^{-1} .

4.2.3. Thermal Analysis

The DTA and TGA curves of SO-3 and JUST-4 samples exhibited a different thermal behaviour in accordance with a diverse mineralogy (Figure 9). SO-3 sample showed an intense endothermic peak at $99\text{ }^{\circ}\text{C}$, related to the loosely bound water molecules [42,43]. In the case of JUST-4 this peak was located at a slightly lower temperature ($88\text{ }^{\circ}\text{C}$) and has a shoulder at $58\text{ }^{\circ}\text{C}$. This could be related to the presence of analcime (7%) in this sample, which has a lower dehydration temperature ($70\text{--}80\text{ }^{\circ}\text{C}$) compared to montmorillonite [44]. The second endothermic peak is associated with the loss of hydroxyl groups of bentonites at about $620\text{ }^{\circ}\text{C}$. In JUST-4, this sharp endothermic peak is absent. Instead, a broad and weak

peak with a maximum in 516 °C can be observed. In analcime, this second endothermic peak was described in a broad temperature interval between 200 and 500 °C [44].

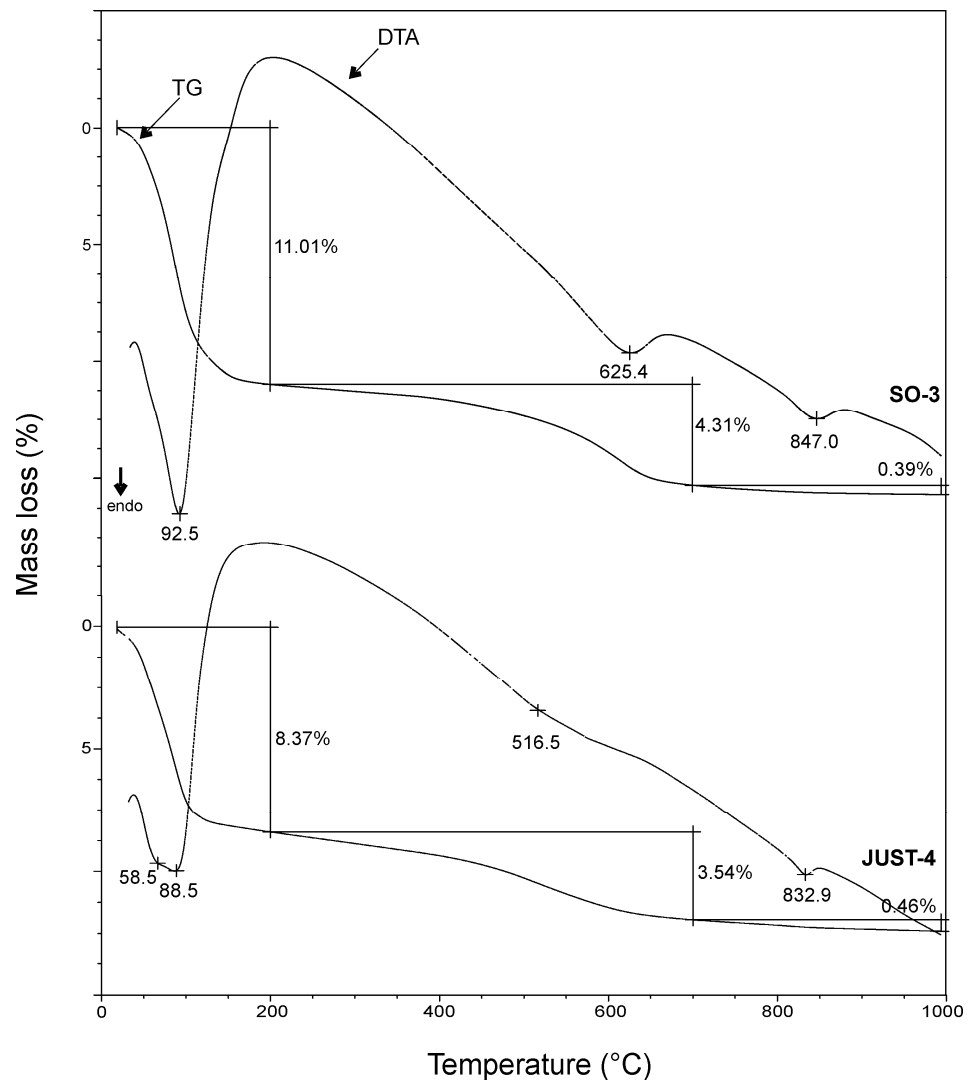


Figure 9. DTA and TG curves of one representative bentonites (SO-3) and one silty claystone (JUST-4) from Justina deposit.

All samples show a low intense endothermic peak at around 850 °C that is related to the destruction of the clay mineral structure. The samples showed the mass loss in two steps mainly. The first mass loss below 200 °C was about 11% in SO-3, while in JUST-4 was only of 8%. The second step mass loss (around 4%) started at around 520 °C and decreased gradually up to 680–700 °C in SO-3. In JUST-4, this step mass loss is broader starting at 400 °C and decreasing up to 700 °C. Total mass loss of SO-3 was higher than JUST-4, which can be related to a higher percentage of phyllosilicates in the former.

4.2.4. Optical Microscopy

The study of the grain mounts from the 0.125 mm granulometric fraction (fine sand) showed the following relative abundance ordering: lithics > biotite > quartz > plagioclase > fibroradial aggregates of quartz > volcanic glass > K feldspar > opaque minerals. Most ubiquitous lithics are andesite grains with hialocrystalline, hialophitic texture matrix where plagioclase phenocrysts are hosted within volcanic glass (Figure 10A). Micas are biotite type, greenish, with anhedral to subhedral grains. Quartz is present as anhedral, subrounded grains with fluid inclusions and undulose extinction; embayments are rare. Plagioclase

is identified as andesine or labradorite with subrounded grains (Figure 10B). Microcline can be observed very subordinate (Figure 10C). Fibroradial quartz is in anhedral and subangular grains resembling calcedonite. It is noticeably the presence of uncoloured, irregular, and angular glass shards (Figure 10D).

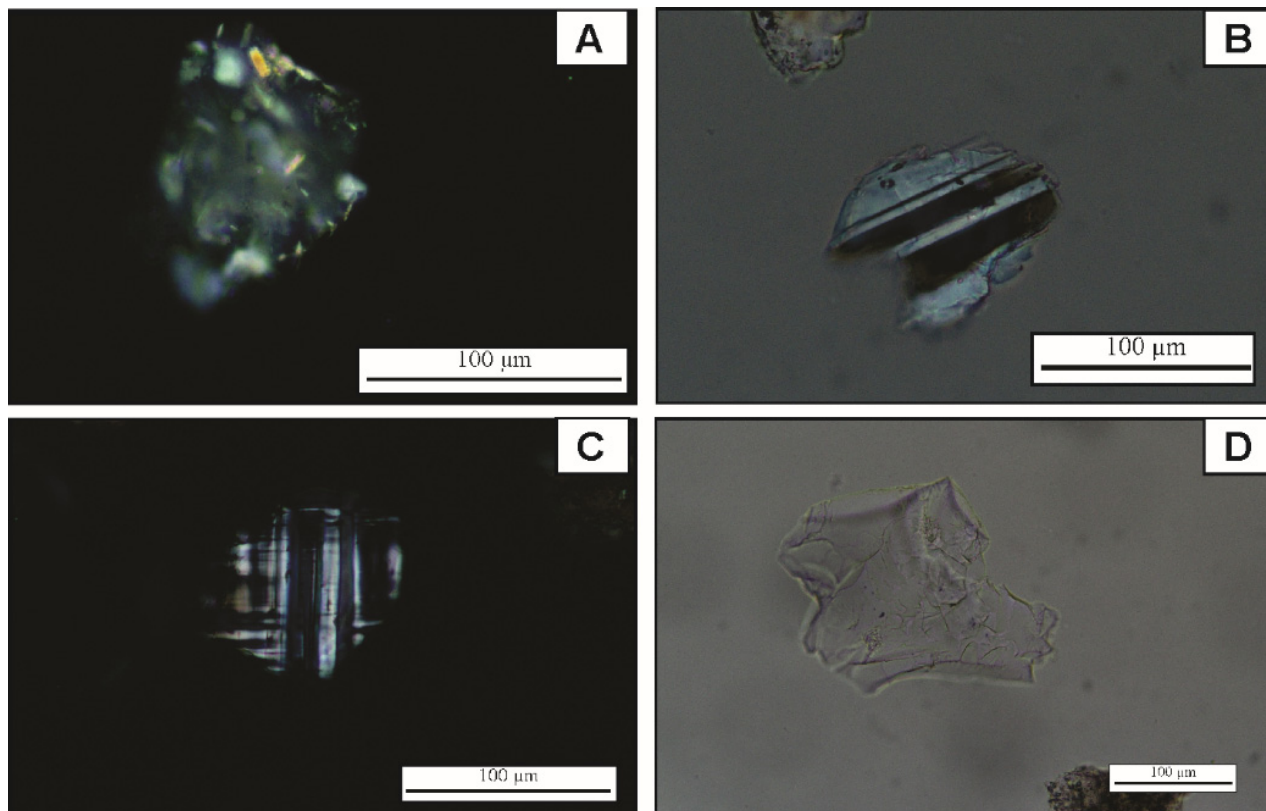


Figure 10. Optical microscope pictures of grain mounts from the 0.125 mm fraction (fine sand) of the bentonites. (A) Plagioclase phenocrysts hosted within volcanic glass. (B) Plagioclase grain. (C) Microcline grain; (D) Angular glass shard.

4.2.5. Scanning Electron Microscopy

SEM study of five selected samples (B-12, JUST-3, JUST-4, and unpublished results of B-12 and JUST-2) confirmed the presence of the minerals identified by means of DRX but also allowed to identify other new phases. Table 4 shows the minerals identified through SEM-EDX with the indication of grain sizes, whereas Table 5 reports representative SEM-EDX analysis of some identified minerals.

Table 4. Minerals identified through SEM-EDX with the indication of grain size. Phlo: Phlogopite, Bt: biotite, Mnt: montmorillonite, Hl: halite, Qz: quartz, Ab: albite.

Sample	Mineralogical Association *
B-12 (bentonite)	Mnt, Phl-Bt, Clt, Fe-Ti oxide, Hl, Ap
SO-4 (bentonite)	Mnt, Phl-Bt, Brt, Ap, Gp, Anl
JUST-2 (bentonite)	Mnt, Phlo-Bt
JUST-3 (bentonite)	Mnt, Phlo-Bt, Gp
JUST-4 (silty claystone)	Mnt, Phlo-Bt, Clt, Ap, Mnz, Zrn, Fe-Ti oxide, Qz, Ab

Table 4. Cont.

Mineral	Sizes
Mica (Phlo-Bt)	50–180 μm
Zircon (Zrn)	12–40 μm
Monazite (Mnz)	16 μm
Analcime (Anl)	6–10 μm
Hematite (Hem)	8–10 μm
Fe-Ti oxide	3–40 μm
Celestine (Clt)	8–25 μm
Barite (Brt)	5–12 μm
Gypsum (Gp)	6–65 μm
Apatite (Ap)	1–10 μm

* Abbreviations of [45].

Table 5. Representative SEM-EDX analysis of some identified minerals.

Analysis	Sample	Na	Mg	Al	Si	Ca	Fe	S						
1	B-12	6.22	8.69	22.3	61.55		1.24							
2	B-12	6.47	9.22	22.7	60.62		0.99							
3	B-12	6.2	9.61	21.84	60.33	1.15	0.87							
4	B-12	6.4	8.43	20.29	55.38	4.19	0.99	4.33						
5	JUST-3	5.78	8.6	22.83	61.51		1.29							
6	JUST-3	6.01	8.94	22.39	61.81		0.84							
Analysis	Sample	Na	Mg	Al	Si	Ca	Fe	K	Ti	Mn	P			
7	SO-4	1.26	12.11	22.35	39.85	1.01	14.11	6.7	2.16	0.45				Mica
8	SO-4	1.48	12.71	20.0	36.59	0.74	18.57	7.86	2.47					Mica
9	SO-4	0.60	11.86	20.56	30.52		22.92	10.43	3.11					Mica
10	B-12		13.55	19.28	32.73		19.83	11.33	3.28					Mica
11	JUST-3	2.24	17.7	21.16	37.89		12.32	6.46	2.25					Mica
12	JUST-3	1.77	17.87	20.28	36.22		13.45	7.81	2.6					Mica
13	JUST-3	1.37	18.45	20.19	36.59		12.55	7.92	2.93					Mica
14	JUST-4	1.38	13.41	22.33	40.06	0.61	12.05	7.93	1.69		0.53			Mica
15	JUST-4	1.69	1.76	36.47	45.11		2.06	12.09	0.81					Mica
Analysis	Sample	Na	Mg	Al	Si	Ca	Fe	K	Ti	S	P	Ba	Sr	Mn
16	SO-4	14.82	2.54	23.16	58.58		0.85							
17	B-12	2.9	9.32	5.48	7.81		65.07		8.8					0.63
18	B-12	2.97		2.31	5.81	3.16	82.09			3.66				
19	B-12					0.9				27.8			71.26	
20	SO-4	4.79	4.07	8.67	13.01					35.89		30.25	3.32	

In oriented samples perpendicular to lamination, the smectite is very compacted with the presence of rounded morphologies or pores in the clay groundmass (Figure 11A). In oblique orientation, it can be seen that smectite aggregates have microlamination (<6 μm) with mica inclusions oriented along the cleavage planes parallel to the lamination (Figure 11B). In detail, the smectite shows typical webby morphologies, with a size lower than 4 μm , with a face-to-face arrangement between laminae, but also with face-to-edge domains inside them (Figure 11C). SEM-EDX analysis (Table 5, analyses 1 to 6) shows that besides Si and Al, these smectites have a high Mg and Na content, which is consistent with an Na-montmorillonite.

Laminar mica grains are common, being angular to subrounded with sizes ranging from silt to fine-grained sand (Figure 11D). In general, they present clean surfaces with no evidence of chemical alteration. SEM-EDX analysis (Table 5, analyses 7 to 15) shows that the mica is predominantly rich in Mg and Fe with low K contents which is interpreted as corresponding to the phlogopite-biotite series. Only one mica grain analysed at JUST-4 departs from this composition as it has a higher K content and therefore suggests a more muscovitic term.

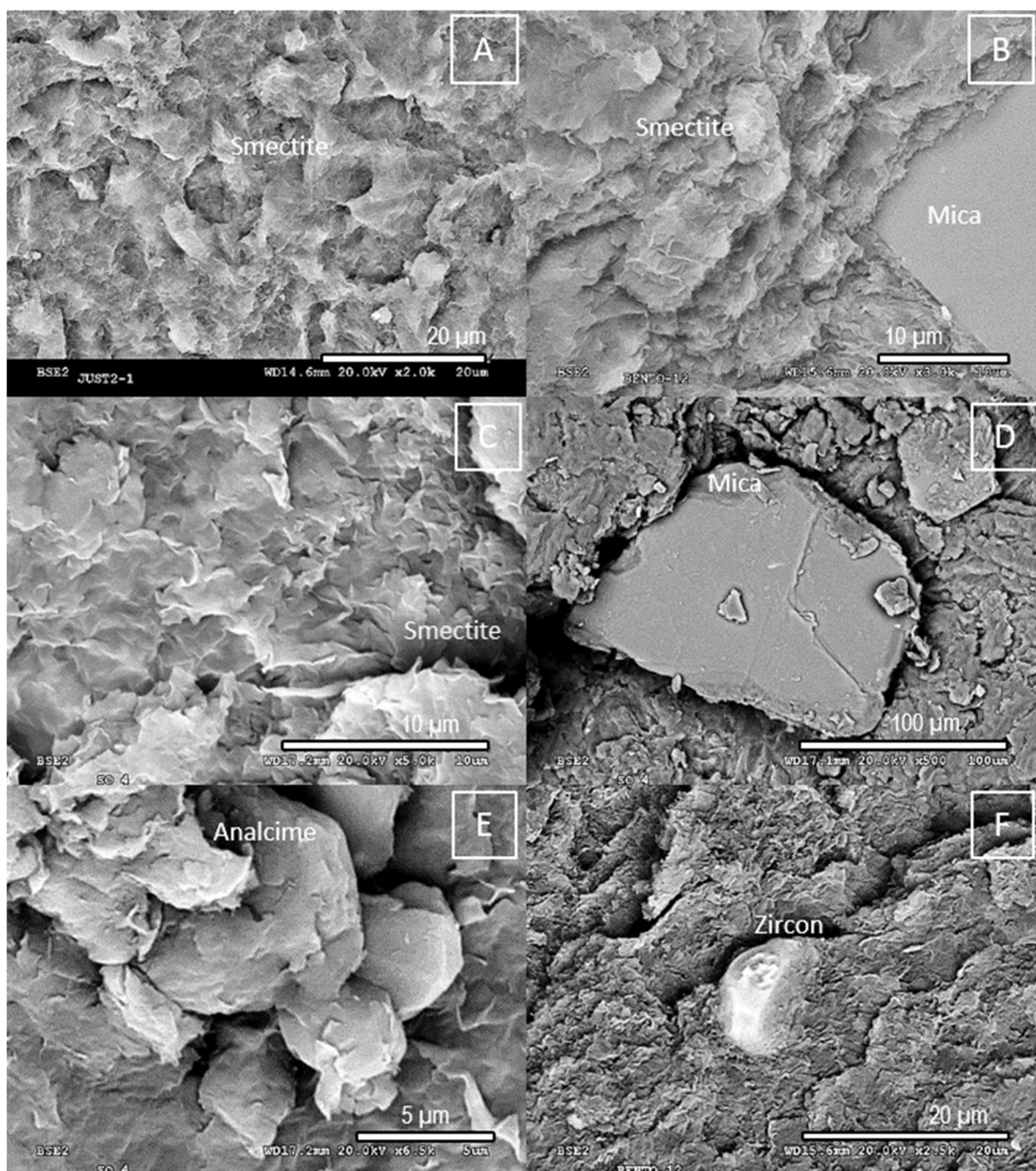


Figure 11. (A) General aspect of bentonite showing compact smectite aggregates where subrounded inclusions and moldic pores are observed (BSE, JUST-1). (B) Laminae microfabric of smectite (sodium montmorillonite) and mica grain parallel to the lamination (BSE, B-12). (C) Detail of the smectite showing the typical crenulated appearance and wrinkling (BSE, SO-4). (D) Subrounded mica grain (phlogopite-biotite) included in the clay groundmass (BSE, SO-4). (E) Small euhedral crystals of analcime included between the smectite aggregates (BSE, SO-4). (F) Euhedral zircon grain included in the clay groundmass (BSE, B-12). (BSE: backscattered electrons).

Other identified silicates are zircon and analcime. The analcime is present as euhedral to subeuhedral very small crystals (up to 10 μm), filling pores as a cement (Figure 11E, Table 5, analysis 16). Zircon is present in small (silt sized) euhedral grains dispersed in the smectite (Figure 11F).

Gypsum is present around surfaces or as a pore-lining cement growing with different sizes and habits (Figure 12A). Euhedral monacite grains have been also identified

(Figure 12B) as well as Fe and Ti oxides, which could be titanomagnetite (Figure 12C and Table 5, analysis 17). The presence of hematites as very small sized (10 μm) inclusions in the smectite groundmass has been observed in the red bentonites (Figure 12D and Table 5, analysis 18).

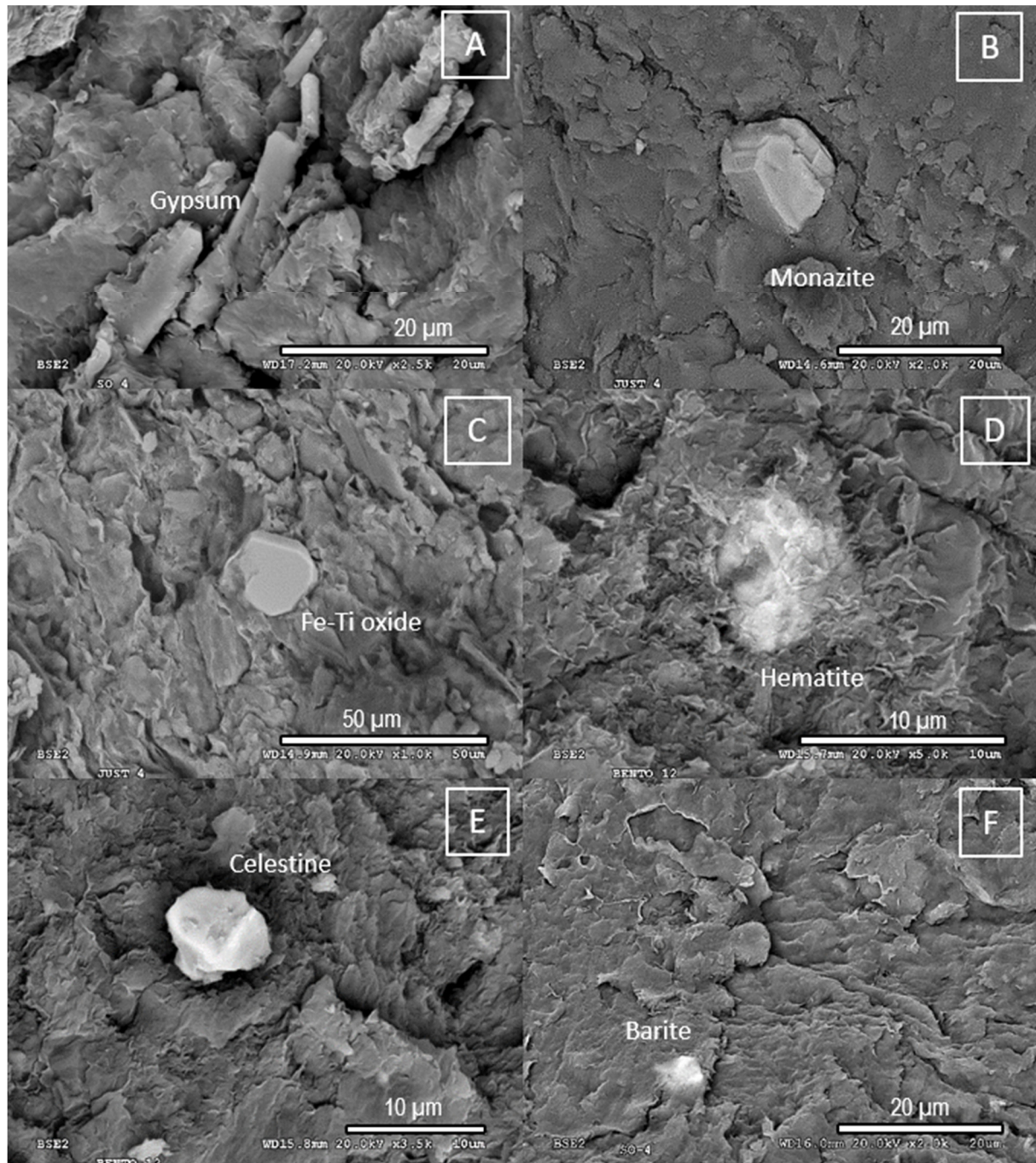


Figure 12. (A) Euhedral gypsum crystals filling pores in the clay groundmass (BSE, SO-4). (B) Euhedral monazite grain (BSE, JUST-4). (C) Euhedral grain of iron and titanium oxide (titanomagnetite) (BSE, JUST-4). (D) Occurrence of hematite in the clay groundmass of a red bentonite (BSE, B-12). (E) Euhedral celestine crystal (BSE, B-12). (F) Barite crystal included in the clay groundmass (BSE, SO-4).

It is noticeably the presence of celestine and barite as small sized (<30 μm) euhedral crystals, which are disseminated or cementing pores (Figure 12E,F, Table 5, analysis 19 and 20). Locally, traces of halite have been identified by SEM-EDX (Table 4).

4.2.6. Texture and Microfabric

Petrographic examination (thin section) of a representative bentonite sample (JUST-2) shows a lamination constituted by laminar mica grains and by relict laminas, sometimes broken, with a dirty appearance (Figure 13A). In other cleaner zones, clay aggregates seem to replace a previous material through lenticular morphologies (Figure 13B). Inside the laminated structure, thicker laminae (25 μm) with different texture and non-oriented morphologies have been recognized (Figure 13C). In detail, two smectite types with different aggregate size have been observed. The smaller particles seem to evolve into larger aggregates by recrystallization leading to zones with a higher birefringence (Figure 13D). The mica is greenish confirming that it belongs to phlogopite-biotite series, some of them with ragged edges, reaching sizes up-to 180 μm (Figure 13E). Some quartz grains and possible glass fragments are detected (Figure 13F). The presence of euhedral opaque crystals is recognized in small aggregates. Opaque minerals with dendritic habits suggest the presence of iron and manganese oxides. Secondary fibrous gypsum has been also identified as surface coatings (Figure 13F).

SEM analysis showed a matrix type microfabric, confirming the presence of two groups of smectites with different particle size. The larger smectites have globular flower-like morphology, reach a size of 20 μm , and seem to originate from the smaller ones (Figure 14A). Included in the smectite groundmass are recognized morphologies with evidence of volcanic composition such as Fe-Ti oxides inclusions (Figure 14B). Besides mica and gypsum crystals, granular aggregates and thin laminar crystals with face-edge and edge-edge arrangements have been observed related to pores (Figure 14C). In samples from Assemblage 2 can be identified the presence of small grain-size zeolites (analcime) and gypsum (<20 μm) infilling porosities (Figure 14D). In the silty claystone to the top of the bentonite level (JUST-4), a matrix-skeletal microfabric with abundant detrital grains of different size can be recognized. The grains are included in a mainly smectitic clay groundmass with possible volcanic glass remains (Figure 14E). Bioturbation features are recognized by the presence of clay filling pedotubules of around 30–40 μm diameter, commonly with celestine euhedral crystals within them (Figure 14F).

4.3. Chemical Composition

Chemical composition of the samples is in accordance with the identified mineralogy (Table 6). The most abundant oxides are SiO_2 (55.18–55.77%) and Al_2O_3 (15.78–16.54%) but Justina bentonites also exhibit a relatively high MgO (5.24–5.84), Na_2O (3.2–4.03) and Fe_2O_3 (1.21–2.08) content. Regarding CaO (0.28–1.14%), K_2O (0.23–0.58%), TiO_2 (0.13–0.19%), P_2O_5 ($\leq 1\%$) and MnO (<0.1%) are present in minor quantities. There are some remarkable differences between chemical composition of Justina bentonites and Pellegrini Lake green bentonites (PEL). For instance, Justina bentonite has lower SiO_2 , Al_2O_3 and Fe_2O_3 content but higher MgO, Na_2O and K_2O content that would indicate a different genesis for each deposit. Compared to continental Triassic bentonite from Cuyana basin (C3) [8], Justina bentonite has lower Fe_2O_3 and Al_2O_3 content but higher MgO and Na_2O content.

Rare earth elements (REE) show that Justina bentonite has lower LREE (La-Gd) and higher HREE (Tb-Y) content compared to PEL bentonite. Total REE content (50.3–67.9 ppm) is slightly lower than PEL bentonite (69.7 ppm). However, these amounts are quite lower than C3 bentonite that has a total REE + Y content of 273.14 ppm (Table 6).

Transition trace elements (TTE-Co, Ni, Cu, Cr y V) are more abundant in Justina bentonites, except for Zn which is higher in PEL bentonite. Analyzing high field strength elements (HFSE), Justina bentonites have higher Nb and Y, similar Ta and lower Zr and Th content than PEL bentonite. In a similar way to the observed with the REE, C3 Triassic bentonite exhibits a higher Zr, Nb, Th, and U content compared to Cretaceous bentonites from Justina and Pellegrini Lake.

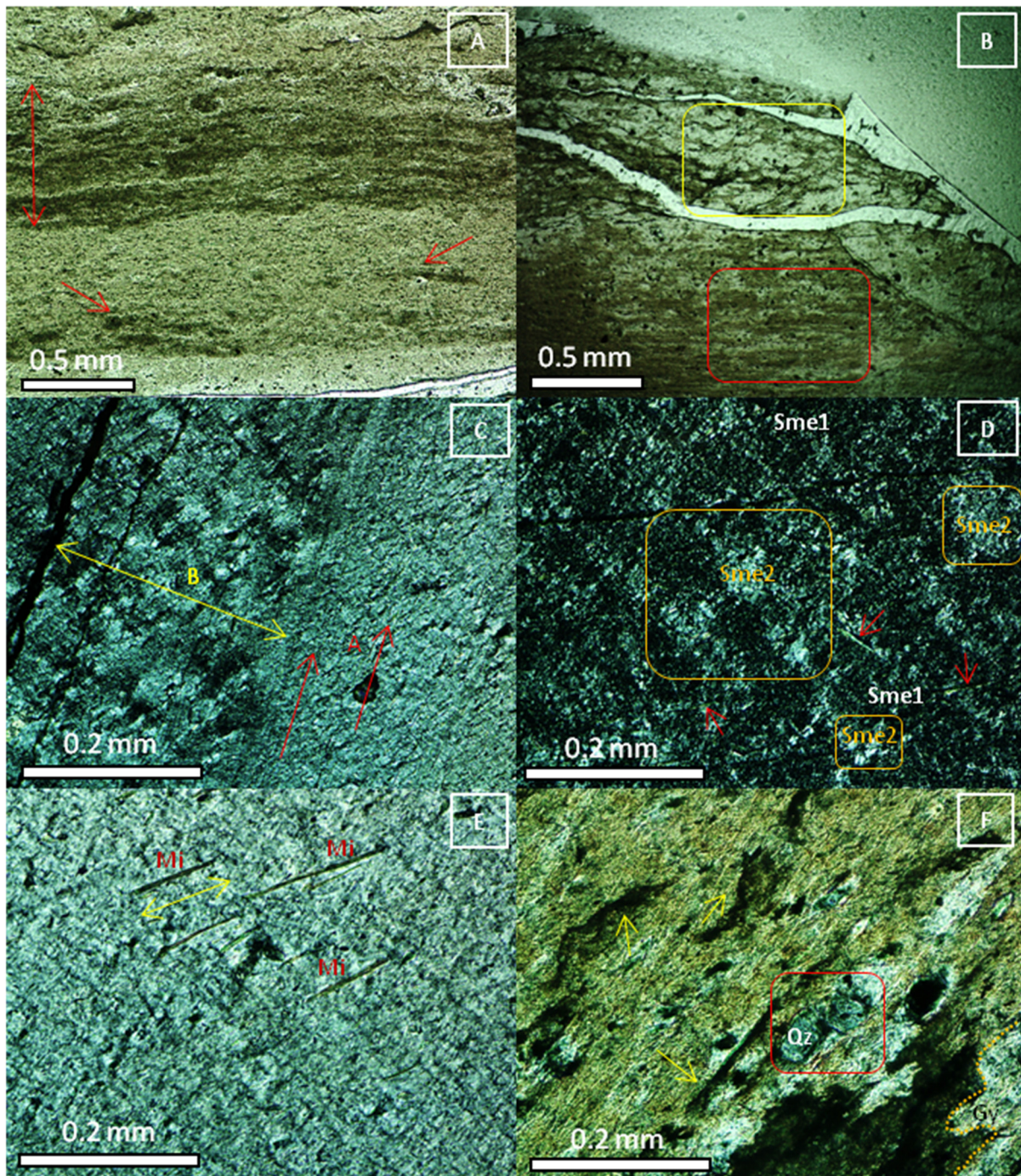


Figure 13. (A) Laminated texture of the bentonite where intraclasts and broken laminae (red arrows) relics of the precursor volcanic ash are observed (PPL). (B) Contact between the dirty-looking laminated texture and the formation of clean lenticular morphologies affecting the laminae (PPL). (C) Textural changes in the bentonite laminations. In A, lamination is emphasized by mica flakes, while in B, smectite aggregates are disoriented (XPL). (D) Two textural types of smectite of different size and birefringence have been recognized: Sme1 and Sme2. Sme2 would be the result of recrystallisation of Sm1 (XPL). (E) Micras (phlogopite-biotite) mark the orientation of the lamination in the bentonite and would be non-bentonitized mineral remains (XPL). (F) Volcanic ash relics in the bentonite (yellow arrows), gypsum (Gy), and quartz grains (red rectangle) have also been identified (XPL). Mi: mica.

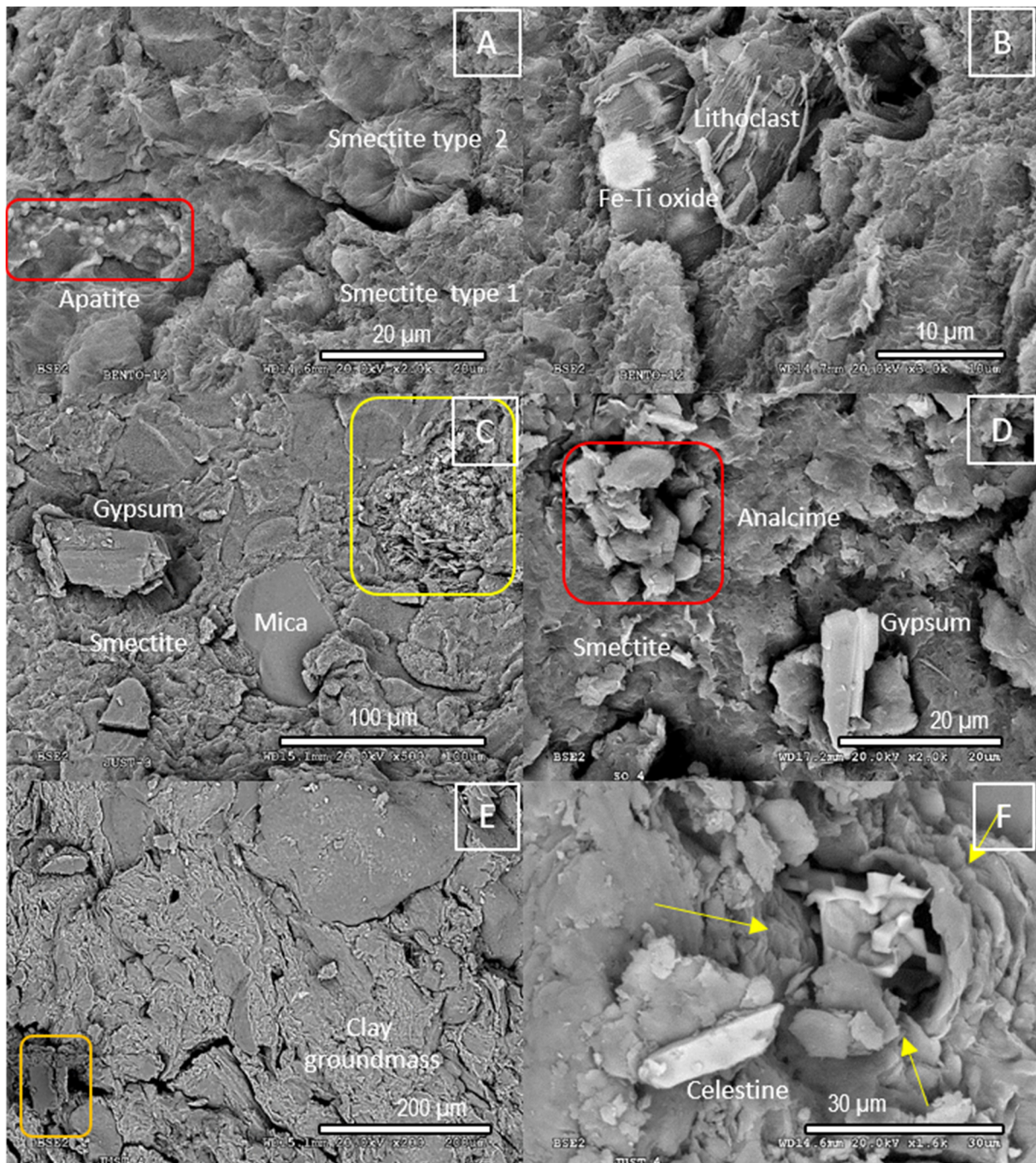


Figure 14. (A) Morphological features of the two types of smectite identified. Type 1 smectite is smaller in size and is interpreted as early. The type 2 smectite shows larger size and flower-like appearance and is later. Small euhedral apatite crystals (red rectangle) are also observed (BSE, B-12). (B) Inclusion in the smectite groundmass of a lithoclast of possible volcanic origin containing Fe and Ti oxide (titanomagnetite) (BSE, B-12). (C) Unidentified debris altered to lamellar minerals (yellow rectangle) in the presence of gypsum and mica (BSE, JUST-3). (D) Pore growth of euhedral crystals of analcime (red rectangle) and gypsum (BSE, SO-4). (E) Skeletal microfacies with frequent terrigenous mineral grains in the clay mass in which traces of possible volcanic glass have been identified (yellow rectangle) (BSE, JUST-4). (F) Euhedral celestine crystals filling root bioturbation pores (yellow arrows) (BSE, JUST-4).

Table 6. Major oxide (wt.%) and trace element (ppm) concentrations of the Justina bentonites (B), Pellegrini Lake bentonite (PEL) and Triassic bentonite from Potrerillos Formation (C3).

%	B-1 *	B-3	B-8 *	B-11	B-12 *	PEL	C3 **
SiO ₂	55.77	54.69	55.18	54.28	55.54	58.13	55.5
Al ₂ O ₃	16.52	15.99	16.54	15.78	16.31	18.48	18.45
Fe ₂ O ₃ (T)	1.42	1.50	1.21	2.08	1.67	3.94	5.38
MnO	0.058	0.058	0.045	0.065	0.074	0.015	0.03
MgO	5.84	5.66	5.76	5.24	5.80	2.90	1.61
CaO	0.49	0.98	0.28	1.14	0.31	0.20	0.76
Na ₂ O	3.20	3.56	3.36	4.03	3.49	2.61	2.46
K ₂ O	0.28	0.36	0.23	0.58	0.26	0.18	0.24
TiO ₂	0.14	0.15	0.127	0.196	0.135	0.145	0.28
P ₂ O ₅	0.10	0.09	0.06	0.08	0.08	0.02	0.04
LOI	16.38	16.56	16.78	15.05	16.33	13.92	N.a
ppm	B-1	B-3	B-8	B-11	B-12	PEL	C3 **
La	9.1	9.9	6.1	9.9	8.2	13.1	45.6
Ce	18.1	18.6	14.2	21.1	17.9	27.1	98
Pr	3.1	3.1	1.8	2.5	2.5	3.4	11.2
Nd	10.3	9.5	6.2	10	7.5	10.4	41.3
Sm	1.9	1.2	1.6	2.1	1.8	1.8	8.21
Eu	0.4	0.4	0.5	0.5	0.4	0.5	0.88
Gd	2.3	2.3	2.7	1.8	1.9	1.9	7.7
Tb	0.3	0.4	0.3	0.5	0.4	0.3	1.33
Dy	2.5	2.4	1.5	2.7	2.2	1.8	7.56
Ho	0.5	0.5	0.4	0.6	0.5	0.4	1.45
Er	1.9	1.1	1.1	1	1.3	0.6	4.64
Tm	0.1	0.2	0.2	0.1	0.1	0.1	0.72
Yb	1.7	1	1.7	1.1	1.4	1.3	5.05
Y	15.7	16	12	12.6	12.4	7	39.5
ppm	B-1	B-3	B-8	B-11	B-12	PEL	C3 **
Co	15.8	12.3	12.4	15.5	16	1.5	
Zn	50	40	40	40	40	90	
Cu	18	23	15	19	28	4	
Ni	20	40	20	30	40	10	
V	166	121	104	74	125	5	5
Cr	60	90	70	80	80	40	20
Zr	53	59	49	61	48	83	223
Nb	17.5	16.6	17.6	15.2	17.6	12.9	20.5
Ta	2.1	1.7	1.8	1.7	2.2	2	1.7
Th	3.5	3.5	3.3	3.9	3.4	6.6	23.1
U	2	2.4	2.5	4.4	3.4	1.8	6.67
Ba	51	48	29	62	44	666	138
Sr	77	133	72	176	65	74	79.2

Table 6. Cont.

ppm	B-1	B-3	B-8	B-11	B-12	PEL	C3 **
Rb	12.5	15.8	8.3	22.6	8.9	10.4	8.5
Cs	1.3	0.8	0.4	2.2	0.4	0.7	2.82
Li	133	127	137	121	132	27	
S	0.09	0.68	0.16	0.71	0.13	0.13	
B	10	10	<10	30	<10	110	
Sc	4	4	4	5	4	4	
Be	2	2	2	2	2	<3	
Ga	22.1	17.2	19.5	19	22.3	20.4	23.3
Ge	1.1	1.6	1.7	1.4	1.6	<0.7	
Mo	2	4	2	4	4	<1	
Pb	14.2	13.5	12.5	11.9	17.2	12.3	
Sn	3.3	2.9	4	2.8	2.5	5.1	

* major elements reported in [17]; ** [8].

With respect to ion lithophile elements (LILE), a significant lower Ba content (<100 ppm) can be observed compared to PEL (>500 ppm) and C3 bentonites. Sr, Rb, and Cs content is variable in Justina bentonites but in general have similar or higher content than the observed in PEL and C3, especially in Sr that can reach values up to 176 ppm.

Li and B stand out from the rest of the trace elements analysed. Justina bentonites are enriched in Li, almost five times higher than PEL (137 ppm). On the contrary, B content in PEL (110 ppm) is ten times higher than Justina bentonite. With respect to the other elements (Sc, Be, Ga, Pb, and Sn) there are no significant differences between them. Finally, Ge and Mo content are slightly lower in PEL bentonite.

5. Discussion

5.1. Paleoenvironmental Interpretation

Spatio-temporal relations between the identified lithofacies allowed the description of 4 facies associations useful for a better understanding and recognition of the sedimentary depositional environments and sub-environments. These associations are laminated sand sheet (LS), sandy bedforms (SB), floodplain fines (FF), and distal overbank deposits (DO). Laminated sand sheet (Sh, Sr) is constituted by sand sheet-like bodies interbedded with thick, muddy sequences that could correspond to distal deposits of larger crevasses splays over floodplain areas [27,46]. Sandy bedforms (Sh, Sp(t), St, Sr) are lenticular and tabular bodies with lateral wedging and a facies arrangement that indicates flow deceleration [47]. They are also interbedded with muddy sequences and are interpreted as channel infill deposits of ephemeral and small channels [27,28]. Floodplain fines are sheet-like bodies with good lateral continuity with a monotonous appearance due to the predominance of massive mudstones lithofacies (Fm) and the subordinated presence of heterolithic lithofacies (Htl). This facies association indicates the predominance of low energy deposits developed over low relief surfaces. According to [27,28], these deposits are characteristics of a muddy floodplain. Distal overbank deposits (Fm, Fl, B) are formed by tabular and laterally wedged bodies interbedded with facies association FF that also interdigitates laterally. Bentonite lithofacies (B) is present as a unique deposit into this facies association. These deposits denote a sedimentation regulated exclusively by decantation processes probably related to ponds. On the basis of the facies association and stratigraphic relation with FF facies, this succession is interpreted as deposited in local depressions of the floodbasin.

Fluvial systems with a predominance of muddy sequences, associated to the development of tabular or sheet bedforms, are related to low relief sedimentation areas affected by the occurrence of sporadic and non-confined low energy flows [48,49]. Since these uncon-

fined sheet floods locate in distal positions of the floodplain as consequence of a decrease of the slope [46], the identified facies associations indicate, for the analysed sedimentary sequences, a distal overbank environment [27]. In this context, the bentonites would have been formed in shallow ponded water body (lake), located in local depressions of the floodbasin that can be only reached by distal overflow deposits. The identified facies and subenvironments have a higher correlation with the observed by [25] in Barreales Sur and Barreales Escondido areas, located to the South of the studied area (Figure 1), where distal overbank deposits predominates in the lower section of Anacleto Formation. An example of Ca-bentonite formation associated with a fluvial context (oxbow lakes) has been cited by [50] in Mid-Miocene deposits from Bavaria (Germany).

In detail, the sedimentary sequence described in JUST profile is representative of the transition from a lacustrine environment to one with subaerial exposure features of a palustrine character within an alluvial-fluvial floodplain context (Figure 5). The presence of bioturbation, reddening and drab haloes indicate pedogenetic processes where water table fluctuations would be responsible of alternating redox conditions. Paleoclimatic indicators suggest that Anacleto Formation was deposited under warm climate with marked wet and dry seasons [25,51]. The occurrence of plant debris associated to bentonites and saline precipitates (e.g., gypsum, halite) support the above mentioned interpretation.

The distribution of the bentonite deposit has an elongated shape with an orientation NNE-SSW. Toward the east, the bed disappears maybe because it corresponds to a lacustrine-palustrine margin, or due to erosional processes or both (Figure 6). The smectite FWHM values (“crystallinity”) also varies with the position of the bentonite being lower (0.49–0.54 2θ) in the central zone and increasing (up to 0.61 2θ) towards the edge of the deposit (Figure 6).

The top of the bentonite bed occurs at different topographic levels in the studied zone. This could be the result of facies distribution, faulting, dipping of the bed, or even the presence of more than one bentonite level, although the last has not been observed in the bore holes. In the field, the beds are horizontal to subhorizontal, therefore a dipping lower than 1° could cause the different position of the top bentonite bed observed. However, taking into account JUST as a reference section, lateral facies distribution could explain not only this displacement of the bed position to the east but also the observed thickness variation.

Considering JUST reference section it is established that bentonites with mineralogical assemblage 1 would be associated to shallow open lacustrine deposits in which millimetric to submillimetric lamination is common (Figure 15), with a well-ordered Na montmorillonite (see FWHM values). Meanwhile, in marginal areas, would be developed palustrine conditions with smectite rich mudstones with a higher content of detrital minerals and subaerial features such as drab haloes and bioturbation. In this case, mineralogical assemblage 2 is typical, that is, Na-montmorillonite poorly ordered than assemblage 1, higher mica and other detrital grains content, and the occurrence of analcime. This can be interpreted as a shallowing upward sequence where palustrine deposits would indicate the change to marginal conditions (palustrine) forming paleosoils that can be occasionally eroded by tractive fluvial deposits. These two associations are very different to that described for detrital fluvial lithofacies (sandstones and mudstones) located below and overlying the bentonite bed. Here, mineralogical assemblage 3 predominates with the predominance of mixed layer illite/smectite(Ca) (R0) and illite, with minor kaolinite/chlorite. Only in JUST 1 sample, from the reference studied sequence, was observed the presence of Na-smectite suggesting that this laminated silty sandstone was deposited early under lacustrine conditions.

5.2. Mineralogical Considerations

The mineralogical assemblages allow to differentiate between inherited and authigenic minerals in the studied materials. Inherited minerals are mainly represented by quartz, mica-illite (biotite-phlogopite, muscovite), mixed layer illite/smectite, chlorite, kaolinite, plagioclase, K-feldspar, monazite, zircon, titanomagnetite, and apatite. Volcanic glass remains (glass shards), and volcanic rock fragments are also included as inherited minerals.

On the other hand, authigenic minerals are mainly represented by Na-smectite, analcime, barite, celestine, gypsum, and hematite. In the bentonites, most of these minerals have a very small grain size ($<75\ \mu\text{m}$), except for the micas that can reach a size up to $180\ \mu\text{m}$ in some of the studied samples. This corroborates that the smectite was formed at the expense of a very fine-grained material previously deposited (e.g., ash).

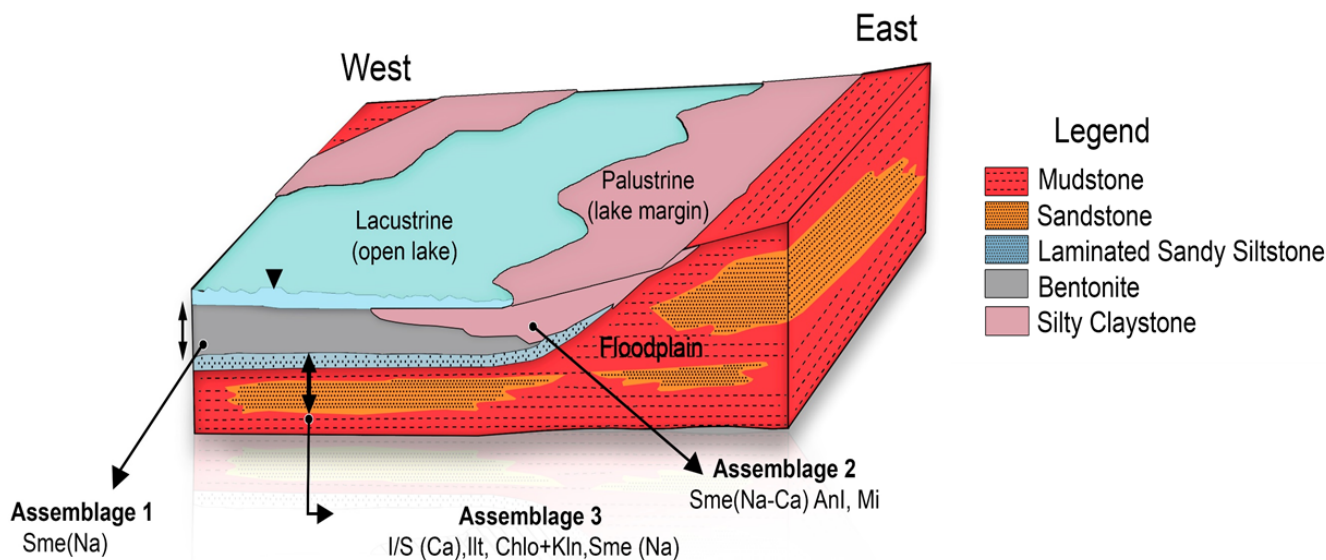


Figure 15. Sketch showing the distribution of mineralogical assemblages in the different sedimentary environments established: lacustrine (assemblage 1), palustrine (assemblage 2), and fluvial (assemblage 3).

This mineralogy is coherent with the results of [52] in the study of coarser facies (sandstones), although some minerals are here cited for first time in the bentonites and associated facies. Is the case of monazite, titanomagnetite, and apatite among the inherited phases and Na-montmorillonite, celestine, and barite within the authigenic phases.

Chemical analyses of micas, based on EDX analysis of the grains, indicate that they belong mostly to the biotite-phlogopite series (Table 5). Only one sample (JUST-4), with more detrital components, has a composition more near to a muscovite member. The relative high proportion of Mg-rich micas could explain the availability of this element in the authigenic Na-smectite.

5.3. Formation of Authigenic Minerals

The spatial and temporal distribution of authigenic minerals in continental settings becomes an important record of paleoenvironmental and paleoclimatic conditions, sensitive indicators of deposition and diagenesis geochemical environment [53].

5.3.1. Dioctahedral Smectite

XRD features of the dioctahedral smectite (main component of the bentonites) show the predominance of Na-montmorillonite in the samples belonging to open shallow lake deposits (samples B and JUST 2 and 3). However, in samples situated in lake margin positions (mostly SO samples) can be observed the presence of Na and Ca, or even only Ca, in the interlayer space. This is very interesting and could indicate that in marginal areas of the lacustrine-palustrine system, the entrance of water with Ca would favors the cationic exchange process in Na-montmorillonite. Other possibility is the incomplete exchange by Na of previous detrital Ca-smectites. The common presence of gypsum, sometimes with a secondary origin, would be evidence of the availability of fluids enriched with the mentioned cation.

This mineralogy has been also corroborated by FTIR and DTA-TGA analyses and show, as it was observed in chemical analysis, the anomalous content of Mg in Justina bentonites

compared with other Mesozoic bentonites as those of Pellegrini Lake deposit. These techniques have also evidenced the absence of significant differences between bentonites (SO-3) and the smectite-rich silty claystone (JUST-4) from a palustrine episode where it is observed a higher detrital content and the presence of zeolites (analcime). EDX chemical analysis have also corroborated a Na-montmorillonite composition rich in Mg. The observed variations are not significant although it has been observed some difference between the obtained analyses of samples B-12 and JUST-3 (Table 5).

Differences in the montmorillonite “crystallinity” were observed as it is evidenced by the FWHM values and crystallite sizes (Figure 6). The lower values (higher crystallite size) are associated to bentonites located in the central zones of the shallow lake and could be the result of smectite recrystallization. Evidence of this process has been observed through petrographic analysis not only in thin section but also in SEM observations. This would be related to the development of different smectite generations during its diagenetic evolution, modifying its textural and microfabric characteristics. These changes could explain the petrographic evidence of thicker laminae with different textures, without the presence of a microlamination inside them (Figure 13). Relict dirty lamination in bentonite samples is related to the existence of a precursor from which originates the clay mineral. The characteristics of some rock fragments identified by SEM and also observed in 0.125 mm granulometric fraction are consistent with the participation of materials with a volcanic origin (e.g., glass, tuff, andesite).

The mineralogical composition of the bentonite contrasts with the mineralogy of the detrital deposits in which is intercalated. The clay fraction of these deposits is rich in illite and mixed layers illite/Ca-smectite, and subordinated chlorite-kaolinite. Therefore, a different source area would be related to these fluvial deposits compared to the lacustrine-palustrine deposits where the Na-montmorillonite is formed.

The formation of bentonites has often been attributed to the chemical alteration of devitrified volcanic ash or volcanic glass, in both continental and marine environments [54,55]. Controls such as the pH, activity of silica, pressure, and temperature have been proposed as the main factors controlling the alteration of the glassy mass and leaching of alkalis that favor the formation of smectites [56,57]. Na-bentonites are linked to environments where the influence of seawater or saline lake water has been considered as the main factor for the incorporation of sodium in the interlayer, whereas Ca-bentonites are more related to continental environments [54–57].

In continental environments, dioctahedral smectite can be formed by the devitrification of volcanic glass in a lacustrine setting and by the chemical weathering of previously deposited volcanoclastic sediments and ophiolitic materials [58]. Additionally, authigenic smectite has been described in salt lakes and sabkha environments [59,60]. Sedimentary processes from the reworking of pyroclastic rocks and deposition of detrital materials in a lacustrine environment can be also result in smectite formation [61]. Another genesis for smectites origin can be from volcanoclastic materials deposited in a shallow lacustrine-palustrine environment during an early diagenetic process [13,14].

In the case of saline-alkaline lakes with a high pH (commonly > 9), chemical parameters such as the silica activity, (Na + K)/H⁺ ratio and cations available from the parental rocks [56,62,63], control the formation of zeolites or smectite.

In the studied materials of the Anacleto Formation, Na-smectite is predominant while zeolite (analcime) is present in low content (<10%) mainly associated with bentonites from the lacustrine-palustrine margin or detrital facies. The interpretation is that during the initial stages of the alteration of the volcanic glass, the (Na + K)/H⁺ ratio was low, favouring the formation of smectite instead of zeolite [64]. The associated fluvial facies providing fresh water support this explanation.

First evidence of the presence of tuffaceous materials in Anacleto Formation were described in the east border of “Bajo de Añelo” depression, in Lomas Coloradas, at 15 km to the SE of the studied area, and in Cerro de los Overos, at 50 km to the NW of the study area [65,66]. Furthermore, tuff levels from the Auca Mahuida Range, very close to the

study area, were assigned to the Anacleto Formation by [25], suggesting that the activity in the magmatic arc and its deposition were synchronic. Consequently, the input of high volumes of fine-grained pyroclastic ashes, as a result of active volcanism, contributed with the formation of continental Cretaceous bentonites in the Neuquén Basin.

5.3.2. Analcime

Generally, there are five main possibilities to explain the formation of analcime in sedimentary environments: (1) forming from precursor alkali zeolites derived from volcanic glass altered in saline alkaline-lake water [67]; (2) from precursors of gels and clay minerals that derived from glass in saline, alkaline lakes [68] (and references therein); (3) direct precipitation from interstitial pore fluids or lake water [69]; (4) formed by the reaction of saline, alkaline pore waters with detrital silicates [69,70]; (5) crystallizing authigenically during the interaction of clay minerals with interstitial brine, however, through an intermediate phase of siliceous gel [71].

Analcime was found at low concentrations (2%) in bentonites located in marginal positions of the lacustrine-palustrine system. The higher percentages were found in the associated facies, which corresponds to the palustrine episode at the top of the bentonite bed where reaches a 7% content. In the analysed samples, this mineral is present as euhedral very small crystals (up to 10 μm) with non-spheroidal habit, filling pores as a cement, outstanding the lack of other zeolites. The absence of spheroidal forms in the analcime indicates that zeolite did not originate from volcanic glass. The spherical forms are indicative of homogeneous nucleation at higher degrees of supersaturation, which is compatible with crystallization from highly reactive volcanic glass in contact with brackish alkaline lake waters [72]. The occurrence of analcime in lacustrine sediments free of associated volcanoclastic material has been reported by a number of researchers [67,68,71,73,74]. In these cases, analcime crystals are subhedral to euhedral, reflecting different chemical conditions for crystal growth than in the volcanoclastic rocks.

Despite the low content of analcime, its formation took place probably by authigenic direct precipitation (neof ormation) or through the reaction between interstitial brines and clay minerals or plagioclase. These mechanisms have been interpreted as being responsible for analcime precipitation in marginal facies of Bogoria Lake, Kenya [74].

In the Anacleto Formation there is evidence of a saline (non-alkaline) lake in which the formation of Na-smectite occurred. The relevance of saline groundwater (Na-rich) and its time of residence so as the existence of pH not strictly alkaline has been pointed out by [71], suggesting a siliceous gel as precursor for analcime precipitation in Lake Lewis, a modern saline lake in Australia. Hence, it is more probable that analcime formation took place by direct authigenic precipitation or through the reaction between interstitial pore fluids and the smectite in an environment of high salinity (high Na content) favored by subaerial exposition.

5.3.3. Barite and Celestine

Barium has a similar ionic radius and electronegativity to potassium and replaces it in many minerals, usually potassium feldspar and micas. In common rock-forming minerals Sr^{2+} substitutes Ca^{2+} (e.g., apatite, pyroxene, plagioclase) [75]. Most barite and celestine has been precipitated from aqueous fluids which contain Ba^{2+} and Sr^{2+} derived from the alteration or dissolution of silicate, carbonate, and/or sulfate minerals in sedimentary, metamorphic, and igneous rocks. They can also form as a result of the replacement of anhydrite or gypsum by interaction with Sr-rich or Ba-rich waters [75].

In the studied area, the existence of arid conditions and saline waters would favor the precipitation of these sulphates sometimes (especially celestine) related with paleosoils development. Celestine formation is more related to evaporitic conditions than barite [76]. According to [77] celestine formation can be the result of syngenetic precipitation from evaporating water or epigenetic replacement of calcium sulphates and carbonates. A third proposal includes formation in relation to microbial environments [78]. Celestine and

barite in the studied samples are present as small sized (<30 µm) euhedral crystals which are disseminated or cementing pores. The euhedral forms and their presence as infillings of pores would indicate an authigenic origin [79]. The presence of feldspars, micas and gypsum in the different facies would justify the supply of Ba and Sr. Their origin was inferred later than the Na-smectite formation.

5.4. Geochemistry of Bentonites

The content of trace elements in the bentonite from Justina shows significant differences with Pellegrini Lake and Potrerillos bentonites. In this sense, Justina bentonites present a marked deficit in REE and B but enrichment in TTE and Li compared to the mentioned bentonites. These differences are related to the parent rock composition from which the Na-smectite was originated. The higher Li abundance implies high salinity conditions, which are not related to marine sources (B depletion) [80].

The REE are elements with limited mobility and fractionation in most geological processes [81]. They are frequently hosted in phyllosilicates and heavy minerals in detrital deposits [82,83]. Their distribution in the sediments depends on the granulometry; clay-rich sediments have a greater capacity to retain these elements, since the constituent clay minerals can incorporate them into their structure and/or adsorb them onto their surfaces [84]. Through the analysis of the REE normalized to chondrite, it is observed that all samples have a similar distribution indicating that their origin is the same [85]. This pattern is also similar to Pellegrini Lake bentonites but different to Potrerillos. Justina bentonites show a less fractionated chondrite-normalized pattern with low LREE/HREE ratios and no or small Eu anomalies which would be related to a less differentiated magma (less felsic) than Potrerillos bentonite [81,86] (Figure 16A).

Bentonite samples were plotted in the bivariate Zr/TiO₂ versus Nb/Y classification diagram of volcanic rocks [87]. Justina and Pellegrini Lake bentonites plot inside trachyandesite field but Potrerillos plot close to the boundary between rhyodacite/dacite and rhyolite confirming that Potrerillos bentonites would have formed from a more evolved magmatism as it is also seen in REE plot (Figure 16B). Although dioctahedral smectites form by alteration of nearly all types of volcanic rocks, trachyandesites are the most suitable precursors [54].

The tectonic discrimination diagrams of [88] based on Rb–Y + Nb, show that the Justina and Pellegrini Lake samples are positioned in volcanic arc granites while Potrerillos plot close to the boundary between arc and interplate granites (Figure 16C).

Proportional values involving comparatively stable elements such as, Th/Co, La/Sc, Cr/Th, and Th/Sc, which have been seen to be reliable markers of source rock determination [86,89,90]. The immobile elements La and Th are more abundant in the felsic rocks than basic ones and the opposite is true for Sc and Co, especially in detrital materials. The Th/Sc ratio is considered to be a good indicator of provenance of magmatic rocks as Th is an incompatible element while Sc is typically compatible during magmatic differentiation [91].

In the present study, these ratios were used to construct binary diagrams with the addition of an intermediate source which falls within the gap between the ratio value ranges of felsic and mafic sources [92,93] (Figure 17A–D). Justina bentonites plot in the domain of mixed source signposting their derivation from mixed rocks; though Pellegrini Lake and Potrerillos fall in the felsic source domain. However, the Th/Sc and Th/Cr ratio show some discrepancies (Figure 17A–C). The Th/Sc values plot in the boundary with felsic source meanwhile Th/Cr values plot closer to the mafic domain. Nevertheless, most REE geochemical data would support a mixed source for Justina bentonites or at least less felsic than Potrerillos and Pellegrini Lake.

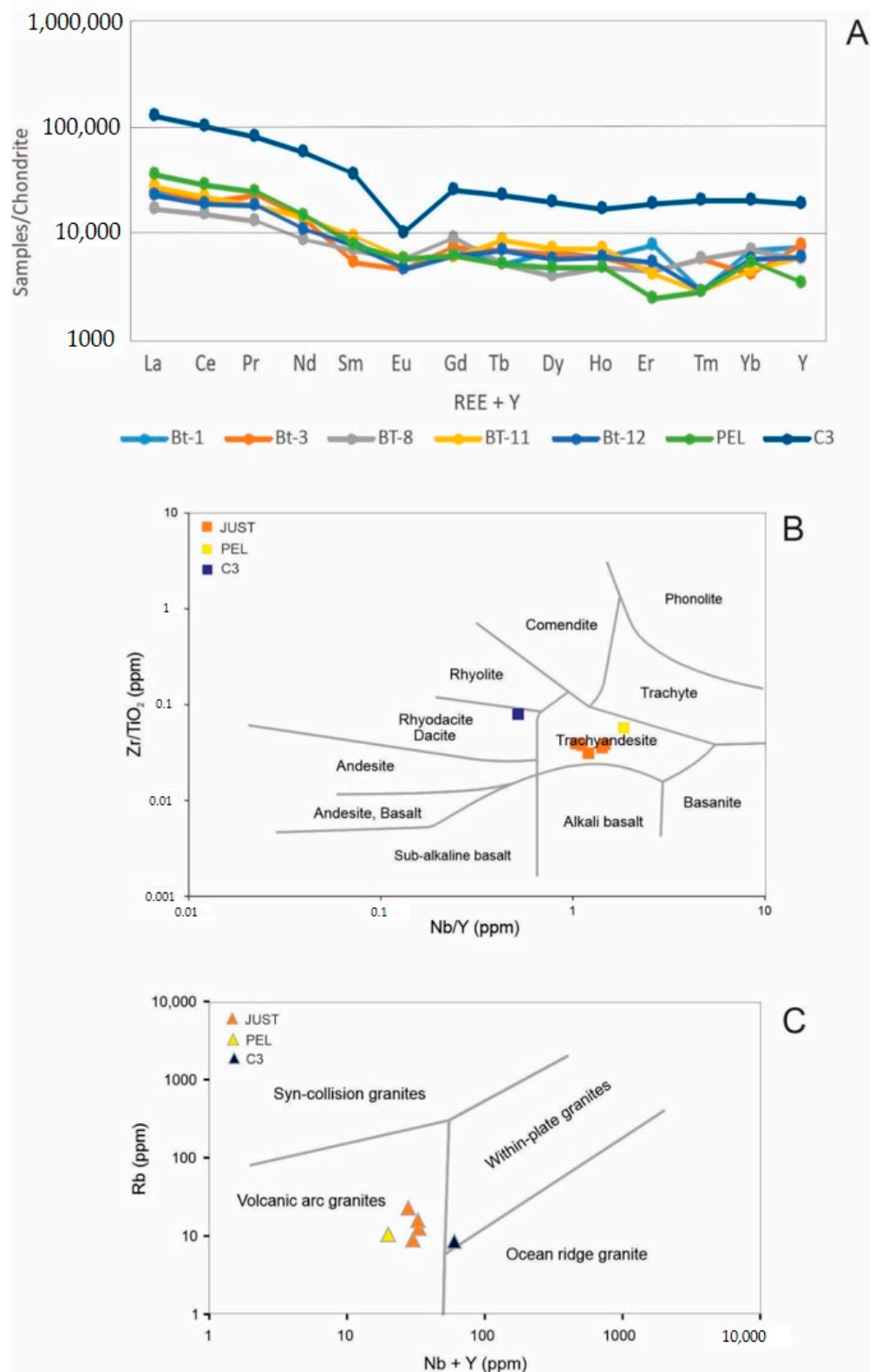


Figure 16. Provenance and tectonic setting geochemistry of Justina bentonites. (A) Chondrite-normalized REE patterns. (B) Bivariate Zr/TiO_2 versus Nb/Y classification diagram of volcanic rocks [87]. (C) Bivariate $Nb + Y$ versus Rb plot [88]. Pellegrini Lake bentonite and Potrerillos bentonite (C3) [8] have been also plotted for comparison.

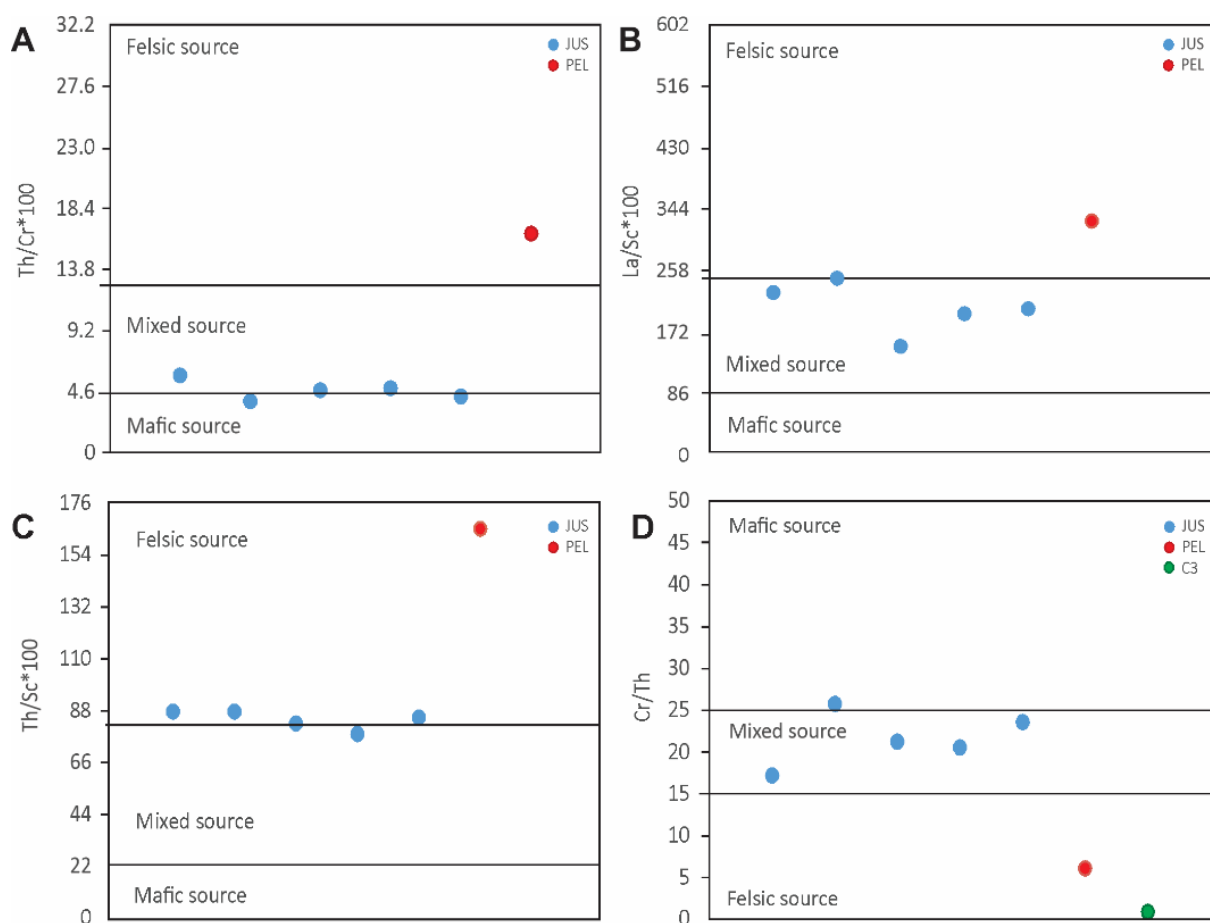


Figure 17. Plots of trace element compositions from the Justina bentonites on the provenance parent rock binary diagrams: (A–D) (Th/Cr, La/Sc, Th/Sc, Cr/Th) (after [92]).

The smectite from Justina deposit could have formed from inherited constituents from both fine fluvial deposits and pyroclastic deposits of tuffs and volcanic glass. Besides the geochemistry of trace elements, the presence of unaltered or partially altered glass shards provides the strongest evidence of a main volcanic precursor developed during early diagenesis. The alteration of volcanic ash to smectite is a hydration reaction that requires magnesium and originates alkali ions and silica. For the bentonitization process, the addition of Mg is necessary especially when the pyroclastic material supplying the volcanic glass is of rhyolitic composition [94]. An intermediate composition of andesitic type is most suitable for smectite formation [54,95]. This explains the importance of seawater (Mg supply) in the formation of bentonite from rhyolitic volcanic glass [59]. In the Justina bentonite deposit, the Mg supply is favoured by the intermediate (trachyandesitic) character of the pyroclastic constituents, and the release of Mg from the micaceous constituents of phlogopite-biotite composition is also involved.

The alteration reaction from volcanic glass to smectite probably took place soon after deposition (early diagenesis), although the existence of several generations of smectite in the bentonite indicates later diagenetic processes in response to changes in water composition. The scheme of formation of Na-smectite and associated authigenic minerals is shown in Figure 18.

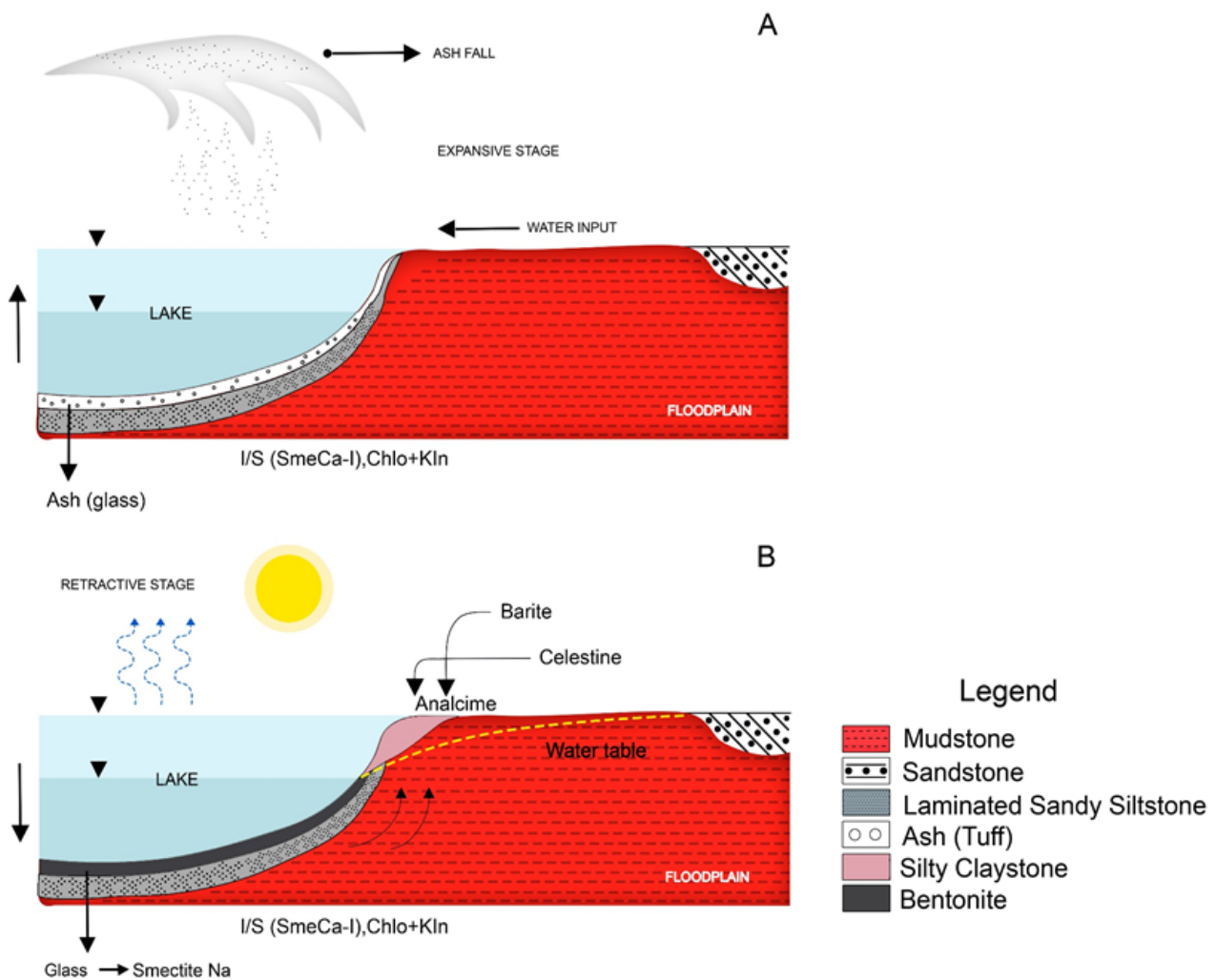


Figure 18. Model of bentonite deposit formation. (A) Expansive (wet) stage of the lacustrine environment because of water and sediment input. The fall ash deposit took place at the bottom of the lake. (B) Retractive (arid) stage caused by the lowering of the lake level and the consequent increase in salinity. The volcanic glass would be diagenetically altered to sodic smectite with lower crystallinity at the lacustrine margin (palustrine). Under these evaporitic conditions, the formation of other authigenic minerals such as analcime, barite and celestine was favored.

According to [96] classification the Justina bentonite belongs to primary distal bentonite deposits formed by in-situ alteration of volcanic and volcanoclastic rocks.

6. Conclusions

The Justina bentonite deposit formed in a very shallow saline lacustrine environment that originated in association with a fluvial floodplain sedimentary setting coinciding with a pyroclastic volcanic event that provided the glassy ash precursor for Na-smectite formation during the Cretaceous (Anacleto Formation).

The smectite is distributed in three mineralogical assemblages in which the smectite is clearly sodic linked to open lake (assemblage 1), calcic to sodic in more marginal areas (assemblage 2) and calcic interstratified with illite (R0) in the siliciclastic facies between which bentonite is intercalated (assemblage 3). Smectite would have formed in early diagenesis from fine-grained pyroclastic material (ashes) in a very shallow and saline lacustrine environment with not high pH conditions (low $(Na + K) / H^+$ ratio) that favoured the formation of Na-smectite instead of zeolites. Texturally, two types of sodic smectite

have been identified with different morphologies and sizes, interpreted as the result of diagenetic recrystallization.

Analcime would have formed later than smectite by direct precipitation (neof ormation) or reaction of saline waters with smectite. The formation of celestine and barite would be caused by the interaction of sulphate-rich waters with strontium and barium ions. Sulphate and Sr could come from the dissolution of gypsum, while Ba would come from the alteration of potassium feldspar or micaceous minerals. The formation of these authigenic sulphates, reported for the first time in Anacleto formation, is later than the formation of smectite.

From a geochemical point of view, the source area of the ashes shows similarities in the Cretaceous bentonites of the Neuquén basin (Justina and Lago Pellegrini) but are very different from those more evolved (felsic) Triassic bentonites of the Cuyana basin (Potrerillo). The differences observed between the bentonites of the Neuquén basin are related to the composition of the waters involved, marine in Lago Pellegrini and evaporitic continental in the case of Justina, which explains the differences in the availability of Li, B and Mg. The pyroclastic input of Justina bentonite would come from a trachyandesitic magmatism tectonically linked to a volcanic arc.

Author Contributions: Conceptualization, T.B.M., G.P. and M.P.; methodology, M.P.; investigation, T.B.M., G.P. and M.P.; resources, A.G.M. and R.G.; writing—original draft preparation, T.B.M., G.P. and M.P.; writing—review and editing, T.B.M., G.P. and M.P.; visualization, M.P.; supervision, M.P.; project administration, G.P.; funding acquisition, G.P., T.B.M. and M.P. All authors have read and agreed to the published version of the manuscript.

Funding: The work is part of the scientific activities of research group GPG-418 (UAM). This research was funded by the Secretaría de Investigación de la Universidad Nacional del Comahue, Argentina, (project 04/I253).

Data Availability Statement: Not applicable.

Acknowledgments: The authors are grateful to TOLSA S.A. for the authorization, information, and supply of the studied samples, and to Monica Sosa for field photographs.

Conflicts of Interest: The authors declare no conflict of interest. The funders had no role in the design of the study; in the collection, analyses, or interpretation of data; in the writing of the manuscript, or in the decision to publish the results.

References

- Eisenhour, F.; Reistch, D. Bentonites. In *Industrial Minerals and Rocks: Commodities, Market, and Uses*; Kogel, S.T., Trivedi, J.E., Barker, N.C., Krobowski, J.M., Eds.; Society for Mining, Metallurgy, and Explorations, Inc.: Littleton, CO, USA, 2006; pp. 357–368.
- Impiccini, A.; Valles, J. Bentonitas. In *Geología y Recursos Naturales de la Provincia del Neuquén*; Leanza, J.M., Arregui, H.A., Carbone, C., Danieli, O., Vallés, J.C., Eds.; Asociación Geológica Argentina: Buenos Aires, Argentina, 2011; pp. 755–762.
- Kramarz, C.; Garrido, A.; Forasiepi, A.C.; Bond, A.M.; Tambussi, M. Estratigrafía y vertebrados (Aves y Mammalia) de la Formación Cerro Bandera, Mioceno Temprano de la Provincia del Neuquén, Argentina. *Rev. Geol. Chile* **2005**, *32*, 273–291. [[CrossRef](#)]
- Barrio, C.A. Paleogeographic control of upper cretaceous tidal deposits, Neuquén Basin, Argentina. *J. South Am. Earth Sci.* **1990**, *3*, 31–49. [[CrossRef](#)]
- Musso, B.T.; Roehl, E.; Pettinari, G.; Vallés, J.M. Assessment of smectite-rich claystones from Northpatagonia for their use as liner materials in landfills. *Appl. Clay Sci.* **2010**, *48*, 438–445. [[CrossRef](#)]
- Andreis, P.E.; Zalba, R.E. Na and K bentonites from Argentina: Composition, origin and age, in A Clay Odyssey. In Proceedings of the 12th International Clay Conference, Bahia Blanca, Argentina, 22–28 July 2001; pp. 41–48.
- Gozalvez, E.; Zappettini, C. *Minerales Industriales de la República Argentina*; Instituto de Geología y Recursos Minerales, Servicio Geológico Minero Argentino: Buenos Aires, Argentina, 2004.
- Salduondo, J.; Comerio, M.; Cravero, F.; Etcheverry, R. Mineralogical and Geochemical Analysis of Sodium Bentonites in Continental Settings: The Uspallata Group (Triassic) of the Cuyana Basin, Mendoza Province. *J. S. Am. Earth Sci.* **2020**, *102*, 102448. [[CrossRef](#)]
- Impiccini, A.; Vallés, J.M. Los depósitos de bentonita de Barda Negra y cerro Bandera, departamento Zapala, provincia del Neuquén, Argentina. *Rev. Asoc. Geol. Argent.* **2002**, *57*, 305–314.
- Anselmi, D.; Panza, G.; Cortés, J.L.; Ragona, J.M. *Descripción Geológica de la Hoja 4569-II El Sombrero, Provincia del Chubut*; Instituto de Geología y Recursos Minerales; Servicio Geológico Minero Argentino: Buenos Aires, Argentina, 2004.

11. Fanti, F. Bentonite chemical features as proxy of late Cretaceous provenance changes: A case study from the Western Interior Basin of Canada. *Sediment. Geol.* **2009**, *217*, 112–127. [[CrossRef](#)]
12. Roberson, H.E. Petrology of Tertiary bentonites of Texas. *J. Sediment. Res.* **1964**, *34*, 401–411.
13. Kadır, S.; Kùlah, T.; Erkoyun, H.; Christidis, G.E.; Arslanyan, R. Geology, Mineralogy, Geochemistry, and Genesis of Bentonite Deposits in Miocene Volcano-Sedimentary Units of the Balıkesir Region, Western Anatolia, Turkey. *Clays Clay Miner.* **2019**, *67*, 371–398. [[CrossRef](#)]
14. Köster, M.H.; Gilg, H.A. Pedogenic, palustrine and groundwater dolomite formation in non-marine bentonites (Bavaria, Germany). *Clay Miner.* **2015**, *50*, 163–183. [[CrossRef](#)]
15. Gopinath, T.R.; Schuster, H.D.; Schuckmann, W.K. Clay mineralogy and geochemistry of continental bentonite and their geological implications, Boa Vista, Campina Grande, PB. *Rev. Bras. Geociências* **1988**, *18*, 345–352. [[CrossRef](#)]
16. Pozo, M.; Galán, E. (Eds.) *Magnesian Clays. Characterization, Origin and Applications*, No. 2; AIPEA Educational Series; Digilabs: Bari, Italy, 2015; p. 380.
17. Musso, T.B.; Pettinari, G.; Pozo, M.; Jalil, M.E.R.; Gil-García, R.G. A new deposit of Na-bentonite from the Upper Cretaceous Anacleto Formation (Neuquén Basin, Argentina): Characterization and properties. *Appl. Clay Sci.* **2022**, *220*, 106461. [[CrossRef](#)]
18. Chiappe, M.; Coria, L.M.; Dingus, R.A.; Jackson, L.; Chinsamy, F.; Fox, A. Sauropod dinosaur embryos from the Late Cretaceous of Patagonia. *Nature* **1998**, *396*, 258–261. [[CrossRef](#)]
19. Ducloux, A.H. Estratigrafía y tectónica de los estratos de dinosaurios del Neuquén. *Boletín Inf. Pet.* **1939**, *16*, 16–17.
20. Roll, A. Über die Ortiz und Roca Schichten des oberen Kreide der Río Negro senke (Nord Patagonien), Neues Jahrb. Für Mineral. *Geol. Und Paläontologie.* **1941**, *85*, 144–190.
21. Cazau, M.A.; Uliana, L.B. El Cretácico superior continental de la Cuenca Neuquina. In *V° Congreso Geológico Argentino*; Asociación Geológica Argentina: Buenos Aires, Argentina, 1973; pp. 131–163.
22. Franzese, J.; Spalletti, L.; Pérez, D.G.; Macdonald, I. Tectonic and paleoenvironmental evolution of Mesozoic sedimentary basins along the Andean foothills of Argentina (32°–54°S). *J. S. Am. Earth Sci.* **2003**, *16*, 81–90. [[CrossRef](#)]
23. Ardolino, L.; Franchi, A.; Fauqué, M. *Geología y Recursos Minerales del Departamento Añelo, Provincia del Neuquén, República Argentina: Escala 1:200.000*; Subsecretaría de Minería de la Nación Dirección Nacional del Servicio Geológico: Buenos Aires, Argentina, 1996.
24. Dingus, J.; Garrido, L.; Scott, A.; Chiappe, G.; Clarkle, L.; Schmitt, J. The litho-, bio-, and magneto stratigraphy of titanosaurian nesting sites in the Anacleto Formation at Auca Mahuevo (Campanian, Neuquén province, Argentina). In *Papers on Geology, Vertebrate Paleontology, and Biostratigraphy in Honor of Michael O. Woodburne*; Museum of Northern Arizona Bulletin; Albright, L.B., III, Eds.; Museum of Northern Arizona: Flagstaff, AZ, USA, 2009; pp. 237–258.
25. Garrido, A.C. Paleoenvironment of the auca mahuevo and los barreales sauropod nesting-sites (Late Cretaceous, Neuquén Province, Argentina). *Ameghiniana* **2010**, *47*, 99–106. [[CrossRef](#)]
26. Pángaro, F.; Martínez, F.; Sattler, R.; Bettini, F. El Bajo de Añelo. In *Geología y Recursos Naturales de la Provincia del Neuquén*; Leanza, J.M., Arregui, H.A., Carbone, C., Danieli, O., Vallés, J.C., Eds.; Asociación Geológica Argentina: Buenos Aires, Argentina, 2011; pp. 399–405.
27. Miall, A.D. *The Geology of Fluvial Deposits*; Springer: Berlin/Heidelberg, Germany, 2006.
28. Miall, A.D. *Analysis of Fluvial Depositional Systems*; Education Course Note Series No 20; American Association of Petroleum Geologists: Tulsa, OK, USA, 1985.
29. Schultz, L.G. Quantitative interpretation of mineralogical composition from X-ray and chemical data for the Pierre Shale. *Geol. Surv. Prof. Pap.* **1964**, *391*, 1–31.
30. Van der Marei, H.W. Quantitative analysis of clay minerals and their admixtures, Contrib. to Mineral. *Petroleum* **1966**, *12*, 96–138.
31. Chung, F.H. Quantitative interpretation of X-ray diffraction patterns of mixtures. I. Matrix-flushing method for quantitative multicomponent analysis. *J. Appl. Crystallogr.* **1974**, *7*, 519–525. [[CrossRef](#)]
32. Moore, J.; Reynolds, D.M. *X-ray Diffraction and the Identification and Analysis of Clay Minerals*, 2nd ed.; Oxford University Press: London, UK, 1997.
33. Grabowska-Olszewska, B.; Osipov, V.I.; Sokolov, V.N. *Atlas of the Microstructure of Clay Soils*, PWN, Warszawa; Państwowe Wydawnictwo Naukowe: Warszawa, Poland, 1984.
34. Harms, J.C.; Fahnestock, R.K. *Stratification, Bed Forms, and Flow Phenomena (With an Example from the Rio Grande)*; Primary Sedimentary Structures and Their Hydrodynamic Interpretation; SEPM Society for Sedimentary Geology: Tulsa, OK, USA, 1965; pp. 84–115.
35. Allen, J.R.L. *Sedimentary Structures: Their Character and Physical Basis*; Elsevier: Amsterdam, The Netherlands, 1982; Volume 1.
36. Farmer, V.; Russell, J.D. The infra-red spectra of layer silicates. *Spectrochim. Acta* **1964**, *20*, 1149–1173. [[CrossRef](#)]
37. Madejová, J.; Komadel, P. Baseline studies of the clay minerals society source clays: Infrared methods. *Clays Clay Miner.* **2001**, *49*, 410–432. [[CrossRef](#)]
38. Madejová, J.; Gates, W.; Petit, S. *IR Spectra of Clay Minerals, in Developments in Clay Science*; Gates, F., Klopogge, W.P., Madejová, J.T., Bergaya, J., Eds.; Elsevier: Amsterdam, The Netherlands, 2017; pp. 107–149.
39. Byrappa, K.; Kumar, B.V.S. Characterization of zeolites by infrared spectroscopy. *Chem. Asian J.* **2007**, *19*, 4933–4935.
40. Abdul-moneim, M.; Abdelmoneim, A.A.; Geies, A.A.; Farghaly, S.O. Synthesis, Characterization of Analcime and Its Application in Water Treatment From Heavy Metal Assiut Univ. *Bull. Environ. Res.* **2018**, *211*, 1–22.

41. Theodosoglou, K.; Koroneos, E.; Soldatos, A.; Zorba, T.; Paraskevopoulos, T. Comparative Fourier Transform Infrared and X-Ray Powder Diffraction Analysis of Naturally Occurred K- Feldspars. *Bull. Geol. Soc. Greece* **2010**, *43*, 2752–2761. [[CrossRef](#)]
42. Peterson, R.; Swaffield, E. Thermal analysis. In *A Handbook of Determinative Methods in Clay Mineralogy*; Wilson, M.J., Ed.; Chapman and Hall: London, UK, 1987; pp. 99–132.
43. Velde, B. The clay perspective. In *Introduction to Clay Minerals*; Springer: Berlin/Heidelberg, Germany, 1992.
44. Sakizci, M. Investigation of Thermal and Structural Properties of Natural and Ion-Exchanged Analcime. No. AFG5 Special Issue. *Anadolu Univ. J. Sci. Technol. A Appl. Sci. Eng.* **2016**, *17*, 724.
45. Whitney, D.L.; Evans, B.W. Abbreviations for names of rock-forming minerals. *Am. Mineral.* **2010**, *95*, 185–187. [[CrossRef](#)]
46. Tunbridge, I.P. Sandy high-energy flood sedimentation—Some criteria for recognition, with an example from the devonian of S.W. England. *Sediment. Geol.* **1981**, *28*, 79–95. [[CrossRef](#)]
47. López Gómez, J.; Arche, A. Architecture of the Cañizar Fluvial Sheet Sandstone Early Triassic, Iberian Ranges, Eastern Spain. *Alluv. Sediment.* **1993**, *17*, 363–381.
48. Allen, J.R.L. A review of the origin and characteristics of recent alluvial sediments. *Sedimentology* **1965**, *5*, 89–191. [[CrossRef](#)]
49. Coleman, J.M. Brahmaputra river: Channel processes and sedimentation, *Sediment. Geological* **1969**, *3*, 129–239. [[CrossRef](#)]
50. Ulbig, A. Investigations on the origin of the bentonite deposits in the Bavarian Upper Freshwater Molasse. *Neues Jahrb. Geol. Palaontol. Abh.* **1999**, *214*, 497–508. [[CrossRef](#)]
51. Holmberg, E. *Descripción Geológica de la Hoja 33d Auca Mahuida, Provincia del Neuquén*; Dirección Nacional de Geología y Minería, Subsecretaría de Minería: Buenos Aires, Argentina, 1964.
52. Armas, P.; Moreno, C.; Sánchez, M.L.; González, F. Sedimentary palaeoenvironment, petrography, provenance and diagenetic inference of the Anacleto Formation in the Neuquén Basin, Late Cretaceous, Argentina. *J. South Am. Earth Sci.* **2014**, *53*, 59–76. [[CrossRef](#)]
53. Hover, V.C.; Ashley, G.M. Geochemical signatures of paleodepositional and diagenetic environments: A STEM/AEM study of authigenic clay minerals from an arid rift basin, Olduvai Gorge, Tanzania. *Clays Clay Miner.* **2003**, *51*, 231–251. [[CrossRef](#)]
54. Grim, N.; Guven, R.E. *Bentonites. Geology, Mineralogy, Properties and Uses. Developments in Sedimentology*; Elsevier: Amsterdam, The Netherlands, 1978.
55. Huff, W.D. K-bentonites: A review. *Am. Mineral.* **2016**, *101*, 43–70. [[CrossRef](#)]
56. Christidis, G.E. Formation and growth of smectites in bentonites: A case study from Kimolos Island, Aegean, Greece. *Clays Clay Miner.* **2001**, *49*, 204–215. [[CrossRef](#)]
57. Galán, R.E.; Ferrel, E. Genesis of clay minerals. In *Handbook of Clay Science*; Bergaya, L.G., Ed.; Elsevier: Amsterdam, The Netherlands, 2013; pp. 83–126.
58. Kadir, S.; Ülah, T.; Önalgil, N.; Erkoyun, H.; Elliott, W.C. Mineralogy, geochemistry, and genesis of bentonites in miocene volcanic-sedimentary units of the ankara-Çankiri basin, central anatolia, Turkey. *Clays Clay Miner.* **2017**, *65*, 64–91. [[CrossRef](#)]
59. Christidis, G.E.; Huff, W.D. Geological Aspects and Genesis of Bentonites. *Elements* **2009**, *5*, 93–98. [[CrossRef](#)]
60. Güven, N. *Smectites, in Hydrous Phyllosilicates: Reviews in Mineralogy*; Bailey, S.W., Ed.; Mineralogical Society of America: Washington, DC, USA, 1988; pp. 497–559.
61. Turkmenoglu, A.G.; Aker, S. Origin of sedimentary bentonite deposits of Cankiri Basin, Turkey. *Sci. Geol.-Mem.* **1990**, *88*, 63–72.
62. Sheppard, B.R.A.; Gude, A.J. Zeolites and Associated Authigenic Silicate Minerals in Tuffaceous Rocks of the Big Sandy Formation, Mohave County, Arizona. USGS Professional Paper 830. 1973. Available online: <https://pubs.usgs.gov/pp/0830/report.pdf> (accessed on 10 April 2022).
63. Iijima, A. Plenary Paper—Geology and Mineralogy: Geology of natural zeolites and zeolitic rocks. *Pure Appl. Chem.* **1980**, *52*, 2115–2130. [[CrossRef](#)]
64. Hay, R.L.; Guldman, S.G. Diagenetic Alteration of Silicic Ash in Searles Lake, California. *Clays Clay Miner.* **1987**, *35*, 449–457. [[CrossRef](#)]
65. Uliana, M.A. *Geología de la Region Compreendida Entre los Ríos Colorado y Negro. Provincias de Neuquén y Río Negro*; Universidad Nacional de La Plata: La Plata, Argentina, 1979.
66. Ramos, V.A. *Descripción Geológica de la Hoja 33c Los Chihuidos Norte, Provincia del Neuquén*; Servicio Geológico Minero Argentino: Buenos Aires, Argentina, 1981.
67. Hay, R. Zeolites and zeolitic reactions in sedimentary rocks. *Geol. Soc. Am. Spec. Pap.* **1966**, *85*, 130.
68. Remy, R.R.; Ferrell, R.E. Distribution and origin of analcime in marginal lacustrine mudstones of the Green River Formation, south-central Uinta basin, Utah. *Clays Clay Miner.* **1989**, *37*, 419–432. [[CrossRef](#)]
69. Campo, M.D.; del Papa, C.; Jiménez-Millán, J.; Nieto, F. Clay mineral assemblages and analcime formation in a Palaeogene fluvial-lacustrine sequence (Maíz Gordo Formation Palaeogen) from northwestern Argentina, *Sediment. Geological* **2007**, *201*, 56–74.
70. Karakaya, N.; Karakaya, M.Ç.; Temel, A. Mineralogical and chemical properties and the origin of two types of analcime in SW Ankara, Turkey. *Clays Clay Miner.* **2013**, *61*, 231–257. [[CrossRef](#)]
71. English, P.M. Formation of analcime and moganite at Lake Lewis, Central Australia: Significance of groundwater evolution in diagenesis, *Sediment. Geological* **2001**, *143*, 219–244. [[CrossRef](#)]
72. Wilkin, R.T.; Barnes, H.L. Nucleation and growth kinetics of analcime from precursor Na-clinoptilolite. *Am. Mineral.* **2000**, *85*, 1329–1341. [[CrossRef](#)]

73. Gall, Q.; Hyde, R. Analcime in lake and lake-margin sediments of the Carboniferous Rocky Brook Formation, Western Newfoundland, Canada. *Sedimentology* **1989**, *36*, 875–887. [[CrossRef](#)]
74. Renaut, R.W. Zeolitic diagenesis of late Quaternary fluviolacustrine sediments and associated calcrete formation in the Lake Bogoria Basin, Kenya Rift Valley. *Sedimentology* **1993**, *40*, 271–301. [[CrossRef](#)]
75. Hanor, J.S. Barite–Celestine Geochemistry and Environments of Formation. *Rev. Mineral. Geochem.* **2000**, *40*, 193–275. [[CrossRef](#)]
76. West, I.M. Vanished evaporites—Significance of strontium minerals. *J. Sediment. Petrol.* **1973**, *43*, 278–279.
77. Hanor, J.S. A Model for the Origin of Large Carbonate- and Evaporite-Hosted Celestine (SrSO₄) Deposits. *J. Sediment. Res.* **2004**, *74*, 168–175. [[CrossRef](#)]
78. Sanz-Montero, M.E.; Rodríguez-Aranda, J.P.; del Cura, M.A.G. Bioinduced precipitation of barite and celestite in dolomite microbialites Examples from Miocene lacustrine sequences in the Madrid and Duero Basins, Spain. *Sediment. Geol.* **2009**, *222*, 138–148. [[CrossRef](#)]
79. Mees, F.; Tursina, T.V. Salt minerals in saline soils and salt crusts. In *Interpretation of Micromorphological Features of Soils and Regoliths*; Stoops, F., Marcelino, G., Mees, V., Eds.; Elsevier: Amsterdam, The Netherlands, 2018; pp. 289–321.
80. Warren, J.K. *Evaporites: A Compendium*; Springer: Berlin/Heidelberg, Germany, 2016.
81. Rollinson, H.; Pease, V. *Using Geochemical Data to Understand Geological Processes*, 2nd ed.; Cambridge University Press: Cambridge, UK, 2021.
82. Mosser, C.; Brillanceau, A.; Besnus, Y. Relationship between sediments and their igneous source rocks using clay mineral multi-element chemistry: The Cenozoic lacustrine Anloua basin (Adamaoua, Cameroon). *Chem. Geol.* **1991**, *90*, 319–342. [[CrossRef](#)]
83. Deer, W.A.; Howie, R.A.; Zussman, J. *An Introduction to the Rock-Forming Minerals*, 3rd ed.; Mineralogical Society of Great Britain and Ireland: London, UK, 2013.
84. Cullers, R.; Barrett, T.; Carlson, R.; Robinson, B. Rare-earth element and mineralogic changes in Holocene soil and stream sediment: A case study in the Wet Mountains, Colorado, USA. *Chem. Geol.* **1987**, *63*, 275–297. [[CrossRef](#)]
85. Lamaskin, T.A.; Dorsey, R.J.; Vervoort, J.D. Tectonic controls on mudrock geochemistry, mesozoic rocks of eastern Oregon and western Idaho, U.S.A.: Implications for Cordilleran tectonics. *J. Sediment. Res.* **2008**, *78*, 765–783. [[CrossRef](#)]
86. Cullers, R. The controls on the major and trace element variation of shales, siltstones, and sandstones of Pennsylvanian-Permian age from uplifted continental blocks in Colorado. *Geochim. Cosmochim. Acta* **1994**, *58*, 4955–4972. [[CrossRef](#)]
87. Winchester, P.A.; Floyd, J.A. Geochemical discrimination of different magma series and their differentiation products using immobile elements. *Chem. Geol.* **1977**, *20*, 325–343. [[CrossRef](#)]
88. Pearce, J.A.; Harris, N.B.W.; Tindle, A.G. Trace element discrimination diagrams for the tectonic interpretation of granitic rocks. *J. Petrol.* **1984**, *25*, 956–983. [[CrossRef](#)]
89. Cullers, R. The geochemistry of shales, siltstones and sandstones of Pennsylvanian-Permian age, Colorado, USA: Implications for provenance and metamorphic studies. *Lithos* **2000**, *53*, 181–203. [[CrossRef](#)]
90. Cullers, R.L.; Podkovyrov, V.N. Geochemistry of the Mesoproterozoic Lakhanda shales in southeastern Yakutia, Russia: Implications for mineralogical and provenance control, and recycling. *Precambrian Res.* **2000**, *104*, 77–93. [[CrossRef](#)]
91. McLennan, S.M.; Taylor, S.R.; McCulloch, M.T.; Maynard, J.B. Geochemical and NdSr isotopic composition of deep-sea turbidites: Crustal evolution and plate tectonic associations. *Geochim. Cosmochim. Acta* **1990**, *54*, 2015–2050. [[CrossRef](#)]
92. Hayashi, H.; Fujisawa, K.; Holland, H.; Ohmoto, H. Geochemistry of ~1.9 Ga sedimentary rocks from northeastern Labrador, Canada. *Geochim. Cosmochim. Acta* **1997**, *61*, 4115–4137. [[CrossRef](#)]
93. Bokanda, E.E.; Fralick, P.; Emile, E.; Betrant, B.S.; Ntoboh, T.C.; Nkongho, A.E.; Cedric, B.B. Geochemical constraints on the provenance, paleoweathering and maturity of the Mamfe black shales, West Africa. *J. Afr. Earth Sci.* **2021**, *175*, 104078. [[CrossRef](#)]
94. Christidis, G.; Dunham, A.C. Compositional variations in smectites. Part II: Alteration of acidic precursors, a case study from Milos Island, Greece. *Clay Miner.* **1997**, *32*, 253–270. [[CrossRef](#)]
95. Christidis, G.E. Do bentonites have contradictory characteristics? An attempt to answer unanswered questions. *Clay Miner.* **2008**, *43*, 515–529. [[CrossRef](#)]
96. Gilg, K.; Kaufhold, H.A.; Ufer, S. Smectite and bentonite terminology, classification, and genesis. In *Bentonites. Characterization, Geology, Mineralogy, Analysis, Mining, Processing and Uses*; Khaufold, S., Ed.; Schweizbart Science Publishers: Stuttgart, Germany, 2020; pp. 1–18.